Production of exotic hadrons in *pp* and nuclear collisions

Jin-Hui Chen[1,2] · Feng-Kun Guo[3,4,5,6] · Yu-Gang Ma[1,2] · Cheng-Ping Shen[1,2] · Qi-Ye Shou[1,2] · Qian Wang[6,7,8] · Jia-Jun Wu[4] · Bing-Song Zou[3,5,6,9]

Abstract

Exotic hadrons, beyond the conventional quark model, have been discovered over the past two decades. Investigating these states can lead to a deeper understanding of the nonperturbative dynamics of the strong interaction. In this review, we focus on the production of exotic hadrons in *pp*, *pp̄*, and nuclear collisions. Experimental observations of light and hypernuclei as prototypes of hadronic molecules in heavy-ion collisions are also briefly discussed.

Keywords Exotic hadrons · Hadron-hadron collision · Heavy-ion collision

1 Introduction

Gell-Mann and Zweig introduced the quark model to classify the hadrons discovered thus far [1, 2]. Mesons and baryons were successfully classified as being composed of $q\bar{q}$, $qq\bar{q}\bar{q}$, etc. and qqq, $qqqq\bar{q}$, etc., respectively, and the lowest-lying states were assumed to be quark-antiquark and three-quark states. Quantum chromodynamics (QCD) introduced dynamics to the quark model, inspiring the construction of constituent quark models with various potentials for quarks and gluons (see, for example, Refs. [3–5]). In consistent quark models, most of the hadrons observed before 2003 could be successfully described in terms of $q\bar{q}$ mesons and qqq baryons, with a few exceptions, such as the lightest scalar mesons, $J^P = 1/2^-$ $N(1535)$, and $\Lambda(1405)$.

Extended author information available on the last page of the article

Consequently, from the quark model perspective, $q\bar{q}$ mesons and qqq baryons are considered ordinary hadrons, whereas those with other possible color-singlet valence contents, defined as quarks and gluons responsible for hadron quantum numbers, are generally called exotic hadrons. These include multiquark states, hybrid mesons and baryons, and glueballs; multiquark states can be further divided into compact multiquarks and hadronic molecules according to how the (anti)quarks are grouped together. For hadronic molecules, the quarks and antiquarks first form color-singlet hadrons, which then interact with each other through the residual strong force to form composite hadronic systems. In this sense, hadronic molecules are not "exotic" but rather a natural extension of atomic nuclei to the composite systems of other hadrons.

Studying how colorful quarks and gluons are grouped inside hadrons is crucial for gaining new insights into the mechanisms of color confinement. Therefore, there have been decades of efforts to search for hadrons with distinct exotic characteristics in experiments, including e^+e^- annihilations, hadron collisions, and electron-ion collisions. Owing to the high statistics of new generations of experiments, many new hadron resonances have been discovered since 2003, with properties at odds with the quark expectations of ordinary mesons and baryons. These are good candidates for exotic hadrons. Most of them are mesonic states observed in the heavy quarkonium mass region and are typically collectively referred to as *XYZ* states.

These exotic hadron candidates have been sought and measured in various experiments. Because QCD is

intrinsically nonperturbative at low energies, it has been challenging to order these experimental observations to gain deeper insights. Various theoretical methods have been used, including lattice QCD, effective field theories, (unquenched) quark models, and QCD sum rules. Each method has its own advantages and drawbacks. Thus far, a universal description of all these exotic hadron candidates is still out of reach. For examples of recent reviews of the experimental observations and theoretical investigations, see Refs. [6–15].

Here, we focus on the experimental observations of exotic hadrons in pp, $p\bar{p}$, and nuclear collisions and discuss the production of exotic hadrons in these collisions. The production of light and hypernuclei as prototypes of hadronic molecules in heavy-ion collisions (HICs) is also briefly discussed.

2 Multiquark candidates with hidden charm and double charm

Above the open-charm threshold, tens of unexpected states with properties that are inconsistent with the expectations of the traditional quark model have been observed since 2003. A few similar states were also observed in the bottomonium mass region. Among these, the Y(mass) states have vector quantum numbers and exhibit strong coupling with the hidden-charm or open-charm final states. The multiquark candidates, including tetraquark Z_Q(mass) and pentaquark P_Q(mass) with a hidden $Q\bar{Q}$ pair, are considered explicitly exotic because they carry nonvanishing isospin and/or strangeness in addition to the $Q\bar{Q}$ pair. Here, Q refers to either a charm or bottom quark.

The first hidden-charm state that triggered studies of exotic states was $X(3872)$, also known as $\chi_{c1}(3872)$, which was observed in the Belle experiment in 2003 [16]. Besides $X(3872)$, $Z_c(4430)$ and $Z_b(10610/10650)$, which were the first charged charmonium- and bottomonium-like states with obvious exotic characteristics, were also observed by Belle [17, 18]. The first vector charmonium-like state $Y(4260)$ and pentaquark states $P_c(4450)$ and $P_c(4380)$ were observed in the BaBar and LHCb experiments [19, 20], respectively.

2.1 Charmonium-like states

$X(3872)$ was discovered by Belle in $B \to K\pi\pi J/\psi$ decays as a narrow peak in the invariant mass distribution of the $\pi\pi J/\psi$ final state [16]. Ten years after its discovery, LHCb performed a full five-dimensional amplitude analysis of $B^+ \to K^+X(3872) \to K^+\pi^+\pi^-J/\psi$ decays and unambiguously yielded the $J^{PC} = 1^{++}$ assignment [21].

The most salient feature of $X(3872)$ is that its mass almost exactly coincides with the threshold of $D^0\bar{D}^{*0}$. The mass and width of $X(3872)$, as given in the latest

version of the Review of Particle Physics (RPP) [22], are (3871.64 ± 0.06) MeV and (1.19 ± 0.21) MeV, respectively. These values were extracted using Breit–Wigner (BW) parameterization. BW parameterization works well only for isolated resonances far from the thresholds of the channels to which the resonance can strongly couple. However, $X(3872)$ is different; thus, the BW width reported in the RPP is not a good approximation of twice the imaginary part of the $X(3872)$ pole position in the complex energy plane.

Using the Flatté parameterization that considers the nearby $D\bar{D}^*$ thresholds [23], the LHCb Collaboration reported the mass and width of $X(3872)$ as $3871.69^{+0.00+0.05}_{-0.04-0.13}$ MeV and $0.22^{+0.07+0.11}_{-0.06-0.13}$ MeV, respectively, using events from b-hadron decays (the pole on the second Riemann sheet is located at $0.06 - i0.13$ MeV relative to the $D^0\bar{D}^{*0}$ threshold) [24]. BESIII reported the mass parameter and imaginary part of the $X(3872)$ pole as $\left(3871.63 \pm 0.13^{+0.06}_{-0.05}\right)$ MeV and $\left(-0.19 \pm 0.08^{+0.14}_{-0.19}\right)$ MeV, respectively, from the processes $e^+e^- \to \gamma X(3872)$, with $X(3872)$ reconstructed from the $D^0\bar{D}^0\pi^0$ and $\pi^+\pi^-J/\psi$ final states [25]. The width from the pole position is significantly smaller than that from BW parameterization.

Although $X(3872)$ was discovered more than 20 years ago, its internal structure remains unclear. The measurement of the absolute branching fraction $\mathcal{B}(X(3872) \to \pi^+\pi^-J/\psi)$ provides useful information regarding its complex nature, in particular, leading to insights into the isospin symmetry-breaking dynamics and possible isospin-1 partners of $X(3872)$ [26]. In 2019, BaBar measured branching fraction $\mathcal{B}(B^+ \to K^+X(3872))$ for the first time with a signal significance of 3σ [27], which made the determination of $\mathcal{B}(X(3872) \to \pi^+\pi^-J/\psi)$ possible by combining known branching fractions as a product, $\mathcal{B}(B^+ \to K^+X(3872))\,\mathcal{B}(X(3872) \to \pi^+\pi^-J/\psi)$, the result of which was $\mathcal{B}(X(3872) \to \pi^+\pi^-J/\psi) = (4.1 \pm 1.3)\%$. The authors in Ref. [28] obtained the absolute branching fractions of six $X(3872)$ decay modes by globally analyzing the measurements from available experiments. In particular, $\mathcal{B}(X(3872) \to \pi^+\pi^-J/\psi)$ was determined to be $\left(4.1^{+1.9}_{-1.1}\right)\%$, and the dominant decay mode was given by $X(3872) \to D^{*0}\bar{D}^0 + $ c.c.[1] with a branching fraction $\left(52.4^{+25.3}_{-14.3}\right)\%$, implying a strong coupling between $X(3872)$ and $D\bar{D}^*$. In addition, the fraction of unknown decays of $X(3872)$ was reported to be $\left(31.9^{+18.1}_{-31.5}\right)\%$. Additional $X(3872)$ decays should be sought in the future.

Because the $X(3872)$ mass is so close to the $D^0\bar{D}^{*0}$ threshold at (3871.69 ± 0.07) MeV [22] and owing to its strong coupling to the $D^0\bar{D}^{*0}$ channel, it was immediately proposed

---

[1] The charge conjugated component "c.c." will be neglected hereafter for simplicity.

that $X(3872)$ is a hadronic molecule of $D\bar{D}^*$ [29] predicted by Törnqvist in Ref. [30]. However, other models, particularly the compact tetraquark model, for which $X(3872)$ is a bound state of the cq diquark and $\bar{c}\bar{q}$ antidiquark [31], are currently being discussed (for reviews, please refer to Refs. [6, 7, 10, 13]).

Another physical quantity under active discussion is the ratio of the partial radiative decay widths to the $\psi(2S)\gamma$ and $J/\psi\gamma$ final states, denoted by

$$\mathcal{R}_{\psi\gamma} = \frac{\Gamma_{X(3872)\to\psi(2S)\gamma}}{\Gamma_{X(3872)\to J/\psi\gamma}}. \tag{1}$$

A recent measurement of $R_{\psi\gamma}$ from LHCb was $1.67 \pm 0.21 \pm 0.12 \pm 0.04$, where the first uncertainty was statistical, the second was systematic, and the third was due to uncertainties in the branching fractions of the $\psi(2S)$ and J/ψ mesons [32]. This result is consistent with previous measurements from LHCb in 2014 [33], Belle in 2011 [34], and BaBar in 2008 [35]. However, it differs from the BESIII result, where the upper limit on the ratio $R_{\psi\gamma} < 0.59$ was set to a 90% confidence level [36]. This discrepancy must be understood in other experiments, particularly Belle II.

The first vector charmonium-like state $Y(4260)$ was observed by BaBar through the initial state radiation (ISR) process $e^+e^- \to \gamma_{\text{ISR}}\pi^+\pi^- J/\psi$ [19]. Subsequently, several Y states, including $Y(4360)$ and $Y(4660)$, were observed at B factories. To study these vector charmonium-like states, BESIII collected large data samples above 4 GeV and reported a precise measurement of $e^+e^- \to \pi^+\pi^- J/\psi$ cross-sections from 3.77 to 4.60 GeV [37]. In the high-statistics analysis by BESIII, the cross-sectional distribution around 4.26 GeV exhibited asymmetry and resulted in a shift in the peak position of $Y(4260)$ to a lower mass. To describe the right shoulder of the $Y(4260)$ line shape, a new BW resonance $Y(4320)$ was introduced; however, this may also be due to the opening of the $D_1\bar{D}$ threshold (see, for example, Ref. [38]). Recently, using data samples with an integrated luminosity of 5.85 fb^{-1}, BESIII measured cross-sections for the process $e^+e^- \to K^+K^- J/\psi$ from 4.61 to 4.95 GeV, where a new vector charmonium-like state $Y(4710)$ was observed [39]. $Y(4710)$ was also confirmed using BESIII in $e^+e^- \to K_S^0 K_S^0 J/\psi$ with a statistical significance of 4.2σ [40]. Thus far, $Y(4710)$ is the known vector charmonium-like state with the highest mass.

$Z_c(4430)^\pm$ reported by Belle in $B \to K\pi^\pm\psi(2S)$ is the first good candidate for an exotic state with a nonzero electric charge [17]. Although it was not confirmed by BaBar by analyzing the same B decays [41], LHCb performed a four-dimensional fit of the decay amplitude for $B^0 \to K^+\pi^-\psi(2S)$ using pp collision data corresponding to 3 fb^{-1} and found that a highly significant $Z_c(4430)^-$ component was required

to describe the data [42]. More charged charmonium-like states, including $Z_c(3900)$ [43, 44], $Z_c(4020)$ [45], $Z_c(4050)$, $Z_c(4025)$ [46], $Z_{cs}(3985)$ [47], $Z_{cs}(4000)$, and $Z_{cs}(4220)$ [48] with a strange quark, have now been observed experimentally. For a precise determination of the $Z_c(3900)$ pole using modern dispersion theory techniques and discussions of this structure, refer to Refs. [49, 50].

Although signals of $Z_c(3900)$ have been reported in $J/\psi\pi$ invariant mass distributions, with the $J/\psi\pi^+\pi^-$ invariant mass in the energy region around $Y(4260)$, by D0 in $p\bar{p}$ collisions through b-flavored hadron decays [51], no statistically significant signals of the $Y(4260)$ and $Z_c(3900)$ states were observed in the prompt production [52].

2.2 Hidden-charm pentaquark and double open-charm tetraquark

The search for pentaquark states has a long history. The first strong experimental evidence of a pentaquark state, referred to as $\Theta(1540)^+$, was reported in the LEPS experiment in $\gamma n \to nK^+K^-$ [53]. However, this finding has not yet been confirmed for the same reaction using larger statistical data samples.

In 2015, LHCb reported the discovery of hidden-charm pentaquark candidates in $\Lambda_b^0 \to K^- p J/\psi$ decay, where the data sample used corresponded to an integrated luminosity of 3 fb^{-1} acquired from 7- and 8- TeV pp collisions [20]. A prominent narrow peak was observed in the pJ/ψ invariant mass spectrum, which was named $P_c(4450)^+$. In the amplitude analysis, a second BW resonance, $P_c(4380)^+$, was introduced to describe the broad bump under the $P_c(4450)$ peak. The significance of these structures was greater than 9σ. Subsequently, LHCb updated this process using Run 2 data with statistics greater by almost one order of magnitude for Λ_b^0 events. They found that in the pJ/ψ mass spectrum, there were three obvious narrow structures [54], one for the pentaquark state $P_c(4312)^+$ and two for $P_c(4440)^+$ and $P_c(4457)^+$, split from the previously observed $P_c(4450)^+$.

As the valence structure of pJ/ψ is $c\bar{c}uud$, the newly discovered particles must be composed of at least five (anti) quarks. Analysis of the LHCb data in Ref. [55] suggests that there is also a 1.7σ significance for a narrow $P_c(4380)$, which differs from the considerably broader value reported by LHCb in 2015 [20]. This analysis is based on the $\Sigma_c^{(*)}\bar{D}^{(*)}$ molecular model, and the existence of such a narrow $P_c(4380)$ is a consequence of the heavy quark spin symmetry. By replacing J/ψ with an η_c meson, LHCb searched for $P_c(4312)^+$ in Λ_b^0 decays, but no evidence was observed [56]. Because the masses of the observed pentaquark states are close to the threshold of a charm baryon and charm meson, LHCb recently scanned 32 final states, including $\Lambda_c^+\bar{D}$,

$\Lambda_c^+ \bar{D}^*$, $\Lambda_c^+ \pi \bar{D}$, $\Sigma_c^{(*)} \bar{D}^{(*)}$, $\Lambda_c^+ D$, $\Lambda_c^+ D^*$, $\Lambda_c^+ \pi D$, and $\Sigma_c^{(*)} D^{(*)}$; however, no significant narrow peak was found for any of the modes.

Two pentaquark candidates with strangeness, $P_{cs}(4459)^0$ and $P_{cs}(4338)^0$, were also observed in the $J/\psi\Lambda$ system in the $\Xi_b^- \to K^- J/\psi\Lambda$ and $B^- \to \bar{p}J/\psi\Lambda$ decays with significance values of less than and greater than 5σ, respectively [57, 58].

Among exotic hadrons, there is a class of hadrons that is particularly interesting: double-charm tetraquarks. Such hadrons have been discussed since the 1980 s (see Ref. [59] for early treatment using the Born-Oppenheimer approximation). The first open-charm tetraquark, $T_{cc}(3875)^+$, comprising $cc\bar{u}\bar{d}$, was discovered in the $D^0 D^0 \pi^+$ invariant mass spectrum by LHCb in 2021 [60, 61]. Its mass was just below the $D^0 D^{*+}$ mass threshold, whereas its width was only a few tens of keV.

3 Production in nuclear collisions

3.1 Existing and future experiments

The high-energy collision of heavy ions is a powerful method for generating extremely hot and dense nuclear matter, often referred to as quark-gluon plasma (QGP) [62–64], which exhibits an energy density comparable to that of the Universe a few microseconds after the Big Bang, with roughly equal numbers of quarks and antiquarks. The extreme energy density of the QGP phase leads to the creation of many strange-antistrange quark pairs from quantum vacuum. As the QGP cools, it transits into hadron gas, resulting in the formation of various baryons, mesons, and their antiparticles. Therefore, these collisions offer a unique opportunity to explore exotic particles such as antimatter, hypernuclei [65–72], and exotic hadrons [73], thereby uncovering important fundamental interactions.

While nuclei are abundant across the universe, antinuclei heavier than the antiproton have only been observed as products of relativistic HICs at facilities such as the BNL Relativistic Heavy-Ion Collider (RHIC) and the CERN Large Hadron Collider (LHC). In these experiments, the time projection chamber (TPC) positioned within a solenoidal magnetic field plays a crucial role in identifying the particles of interest by measuring the mean energy loss per unit track length, $\langle dE/dx \rangle$, as illustrated in Fig. 1. As shown in the left panel, STAR reported the observation of $^4\overline{\mathrm{He}}$, which is the heaviest stable antinucleus detected to date [66]. A total of 18 counts were detected in Au+ Au collisions at center-of-mass (c.m.) energies of 200 GeV and 62 GeV per nucleon-nucleon pair. This discovery came a century after Rutherford first observed alpha particles. The yield also
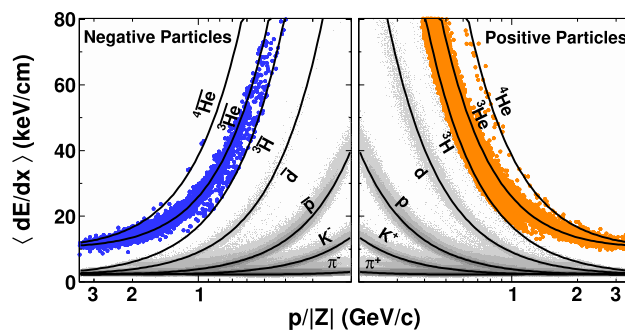

Fig. 1 (Color online) TPC mean energy loss per unit track length, $\langle dE/dx \rangle$ as a function of rigidity, $p/|Z|$, where p and Z are the momentum and charge, respectively. From Ref. [66]

aligns with the predictions from both thermodynamic and coalescent nucleosynthesis models [66].

Hypernuclei are the bound states of nucleons and hyperons and offer valuable insights into hyperon-nucleon interactions. While nucleons (protons and neutrons) are composed solely of up and down quarks, hyperons are light-flavored baryons that contain at least one strange quark. A hypernucleus is defined as a nucleus that contains at least one hyperon in addition to nucleons. Despite being bound within hypernuclei, all hyperons are inherently unstable because they decay via weak interactions. The simplest bound hypernucleus is the hypertriton ($^3_\Lambda\mathrm{H}$) [74], which comprises a Λ hyperon, proton, and neutron. The first hypernucleus was observed in 1952 using a nuclear emulsion cosmic-ray detector [75]. In contrast, the first observation of antihypertritons, which care composed of an antiproton, antineutron, and $\bar{\Lambda}$, was reported by STAR in Au+Au collisions at $\sqrt{s_{\mathrm{NN}}} = 200$ GeV in 2010 [65] through the decay channel $^3_{\bar{\Lambda}}\overline{\mathrm{H}} \to {^3\overline{\mathrm{He}}} + \pi^+$. The measured yields for $^3_{\bar{\Lambda}}\overline{\mathrm{H}}$ and $^3\overline{\mathrm{He}}$ are comparable, indicating a balance in the populations of up, down, and strange quarks and antiquarks in both coordinate and momentum space [65, 71]. This is a consequence of the approximate SU(3) flavor symmetry among the up, down, and strange quarks of QCD.
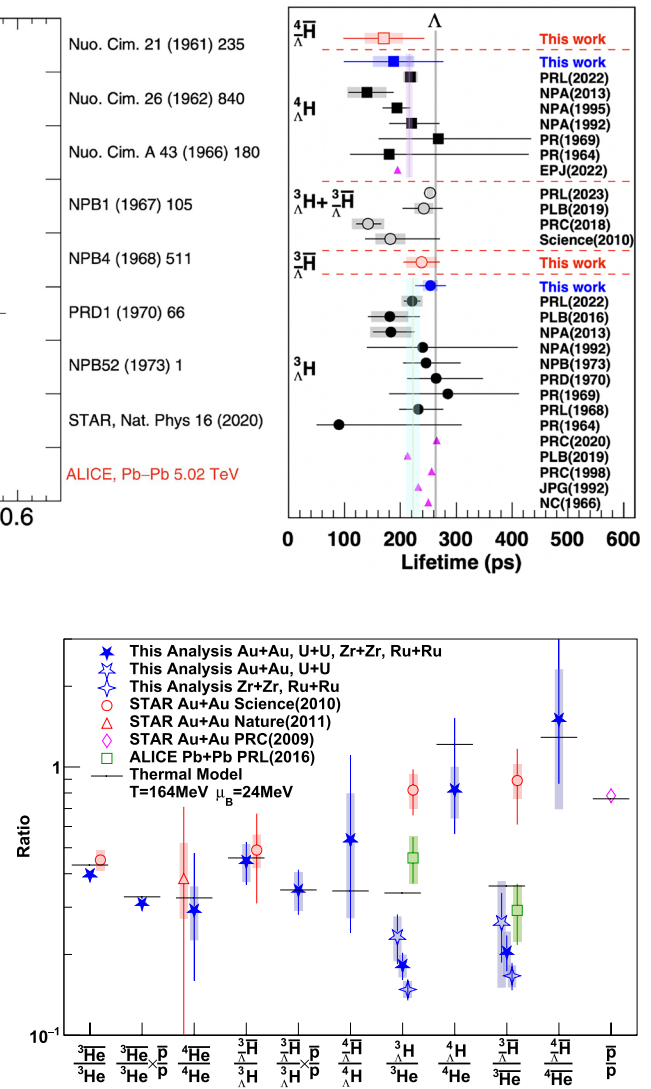
The most precise measurements of the $^3_\Lambda\mathrm{H}$ lifetime (τ) and Λ separation energy (B_Λ) were obtained in Pb-Pb collisions at $\sqrt{s_{\mathrm{NN}}} = 5.02$ TeV at ALICE [76] (c.f. Fig. 2). These measurements are consistent with the predictions from effective field theories and support the characterization of $^3_\Lambda\mathrm{H}$ as a weakly bound system [74]. Although some discrepancies, referred to as the "hypertriton puzzle", have been noted in the literature regarding the lifetime and B_Λ, a global average of all available measurements revealed no significant global tension, with a 23% probability for the lifetime and 57% for B_Λ, as determined by a Pearson test [76]. The upcoming Run 3 of the LHC is expected to provide these measurements with unprecedented precision.

Fig. 2 (Color online) Λ separation energy B_Λ of hypertriton (left) and the lifetime of various hypernuclei (right) measured in different experiments. From Refs. [76] and [71]

Recently, STAR reported the observation of an antimatter hypernucleus, $^4_{\bar{\Lambda}}\overline{\text{H}}$, which consists of an $\bar{\Lambda}$, antiproton, and two antineutrons [71]. This discovery was achieved through two-body decay. A total of 15.6 candidate $^4_{\bar{\Lambda}}\overline{\text{H}}$ antimatter hypernuclei were identified, with an estimated background count of 6.4 [71]. This is the heaviest unstable antinucleus reported to date. The lifetimes of the antihypernuclei $^3_{\bar{\Lambda}}\overline{\text{H}}$ and $^4_{\bar{\Lambda}}\overline{\text{H}}$ were measured and compared with those of their corresponding hypernuclei, thereby providing a test for the symmetry between matter and antimatter. The lifetimes of the (anti)hypernuclei $^3_{\bar{\Lambda}}\overline{\text{H}}, ^4_{\bar{\Lambda}}\overline{\text{H}}, ^3_\Lambda\text{H},$ and $^4_\Lambda\text{H}$ are depicted in Fig. 2. The differences in the lifetimes of hypernuclei and their corresponding antihypernuclei were $\tau\left(^3_{\bar{\Lambda}}\overline{\text{H}}\right) - \tau\left(^3_\Lambda\text{H}\right) = 16 \pm 43(\text{stat.}) \pm 20(\text{sys.})$ ps and $\tau\left(^4_{\bar{\Lambda}}\overline{\text{H}}\right) - \tau\left(^4_\Lambda\text{H}\right) = 18 \pm 115(\text{stat.}) \pm 46(\text{sys.})$ ps. Both differences are approximately zero within the uncertainties, indicating no significant disparity between the properties of matter and antimatter particles, thus providing a new test of CPT symmetry.

Various production yield ratios among (anti)hypernuclei (including hypernuclei and/or antihypernuclei) and (anti)nuclei (including nuclei and/or antinuclei) were assessed and compared with the theoretical models, offering insights into their production mechanisms. As shown in Fig. 3, the antimatter-over-matter particle yield ratios are below unity because the colliding heavy ions carry positive baryon numbers; consequently, the collision system has a positive baryon chemical potential. The data are consistent with most existing measurements within their uncertainties and with the expectation of the coalescence picture of the (anti)nucleus and (anti)

Fig. 3 (Color online) Production yield ratios among the various (anti) nuclei and (anti)hypernuclei with the same number of (anti)baryons measured in heavy-ion collisions. From Ref. [71]

hypernucleus production and statistical thermal model [71]. Relationships between the production yield ratios $^4\overline{\text{He}}/^4\text{He} \approx {}^3\overline{\text{He}}/^3\text{He} \times \bar{p}/p$, $\frac{^4_{\bar{\Lambda}}\overline{\text{H}}}{^4_\Lambda\text{H}} \approx {}^3_{\bar{\Lambda}}\overline{\text{H}}/^3_\Lambda\text{H} \times \bar{p}/p$, $^4_\Lambda\text{H}/^4\text{He} \approx 4 \times {}^3_\Lambda\text{H}/^3\text{He}$, and $^4_{\bar{\Lambda}}\overline{\text{H}}/^4\overline{\text{He}} \approx 4 \times {}^3_{\bar{\Lambda}}\overline{\text{H}}/^3\overline{\text{He}}$ are consistent with the coalescence model of (anti)nucleus and (anti)hypernucleus production. Here, a factor of four in the last two relations arises because both the spin-0 and spin-1 states of $^4_\Lambda\text{H}$ possess sufficiently large binding energies, leading to no energetically allowed strong decay channels. Consequently, the spin-1 state, with a spin degeneracy of three, decays electromagnetically to the spin-0 ground state, enhancing the total production

yields of $^4_\Lambda$H and $^4_\Lambda\overline{\text{H}}$ by a factor of four compared to those of ^{4}He and $^4\overline{\text{He}}$, which have only spin-0 states. Considering this spin-degeneracy effect, the statistical-thermal model predictions align well with the experimental measurements, although the $^4_\Lambda$H/^{4}He ratio is slightly lower than the predicted value. This discrepancy, although not statistically significant, may be attributed to the low binding energy of $^3_\Lambda$H, which suggests that the spatial extent of its wave function is comparable to that of the entire collision system [77].

High-energy pp collisions and HICs provide excellent laboratories for exploring multistrange dibaryons [78–82]. In the search for a possible $\Lambda\Lambda$ bound state, known as the H-dibaryon, femtoscopic correlations of $\Lambda\Lambda$ pairs have been studied in pp, Au+Au, and pPb collisions [83, 84]. By comparing the measured data with model calculations, the scattering parameter space, which is characterized by the inverse scattering length and effective range, is constrained. The data revealed a shallow attractive interaction, which is consistent with the findings of hypernuclei studies and lattice computations.

In addition to antimatter and hypernuclei, HICs also serve as a laboratory for studying hidden-charm XYZ particles. The first evidence of $X(3872)$ production in relativistic HICs was previously reported [85]. $X(3872)$ production in Pb-Pb collisions at $\sqrt{s_{NN}} = 5.02$ TeV was investigated, utilizing the decay chain $X(3872) \rightarrow J/\psi\pi^+\pi^- \rightarrow \mu^+\mu^-\pi^+\pi^-$. The significance of the inclusive $X(3872)$ signal was measured at 4.2 standard deviations [85]. The prompt $X(3872)$ to $\psi(2S)$ yield ratio was found to be $\rho_{\text{Pb-Pb}} = 1.08^{+0.49}_{-0.52}$, which is significantly higher than the typical values of 0.1 observed in pp collisions [85]. For a further discussion, see Sect. 3.3.

Another common observable in the interaction of quarkonium states with the medium created in HICs is the nuclear modification factor R_{AA}, which is defined as the ratio of the yield in central HICs to that in pp collisions, normalized by the number of binary collisions in the reaction. As shown in Refs. [86–89], the suppression of the production yields of $\psi(nS)$ and $\Upsilon(nS)$ mesons in Pb-Pb collisions relative to those in pp collisions was studied using data from the CMS experiment at the LHC, which are summarized in Fig. 4. For the $\psi(nS)$ states, integrated over collision centralities, the nuclear modification factors R_{AA} were 0.56 ± 0.08 (stat.) ± 0.07 (syst.) for J/ψ, 0.12 ± 0.04 (stat.) ± 0.02 (syst.) for $\psi(2S)$, and less than 0.10 (at 95% confidence level) for $\psi(3S)$, revealing sequential suppression [88, 89]. The $\Upsilon(2S)$ and $\Upsilon(3S)$ mesons were also studied [88, 89], with $\Upsilon(3S)$ observed for the first time in Pb-Pb collisions with a significance above five standard deviations. The suppression of Υ yields increased from peripheral to central collisions and

Fig. 4 (Color online) Double ratios among the different $\Upsilon(nS)$ states and nuclear modification factor R_{AA} as functions of $\langle N_{\text{part}} \rangle$. From Refs. [86, 87]
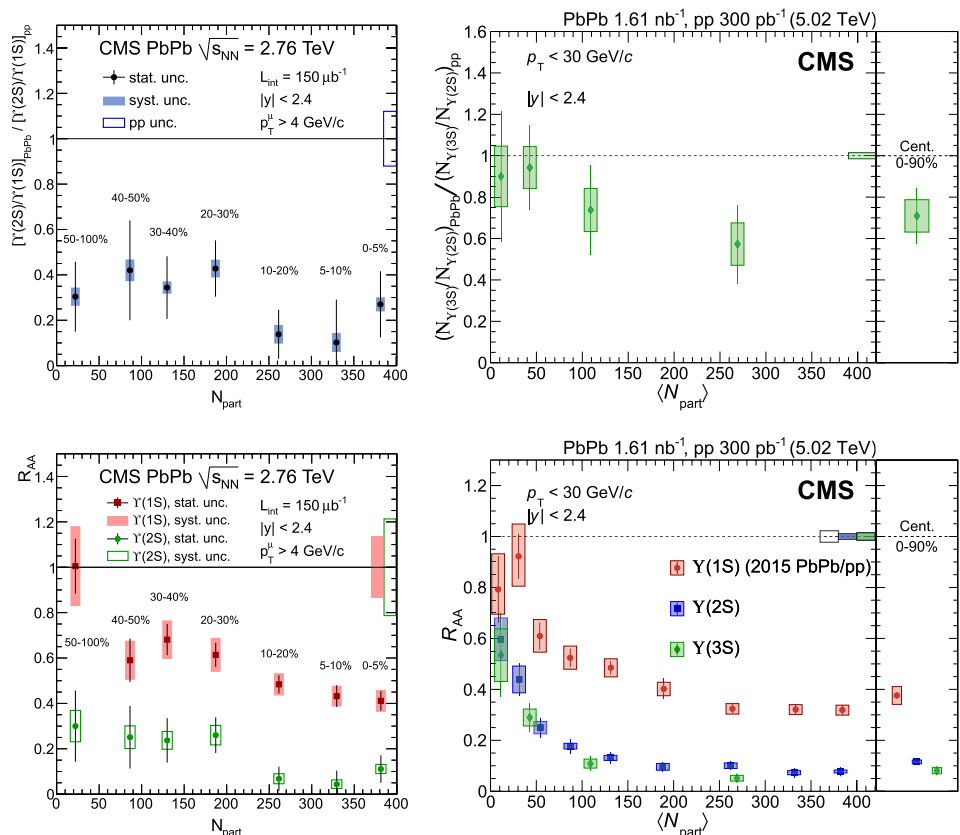
was more pronounced for $\Upsilon(3S)$ than for $\Upsilon(2S)$ (see Fig. 4), extending the sequential suppression pattern previously reported for other quarkonium states.

As reported in Ref. [90], LHCb measured the production of an exotic hadron $X(3872)$ in *p*Pb collisions at $\sqrt{s_{NN}} = 8.16$ TeV [91]. A comparison with the charmonium state $\psi(2S)$ revealed that the dynamics of $X(3872)$ in a nuclear medium differed from those of conventional hadrons. Additionally, compared with proton-proton collision data, the presence of the nucleus may affect the production rates of $X(3872)$ (see Fig. 5). This marked the first determination of a nuclear modification factor for an exotic hadron.

LHCb also measured the feed-down fractions of χ_{c1} and χ_{c2} decays, contributing to the prompt J/ψ yield in *p*Pb collisions at $\sqrt{s_{NN}} = 8.16$ TeV. The results, presented as a function of the J/ψ transverse momentum $p_{T,J/\psi}$ in the range $1 < p_{T,J/\psi} < 20$ GeV, revealed that the fraction at forward speed was consistent with the measurement in *pp* collisions at $\sqrt{s} = 7$ TeV [92] (see Fig. 6). However, the fraction at backward rapidity was 2.4σ higher than that at forward rapidity for $1 < p_{T,J/\psi} < 3$ GeV. This increase at low $p_{T,J/\psi}$ in the backward region aligns with the observed suppression of $\psi(2S)$ contributions to the prompt J/ψ yield. Additionally, the study placed an upper limit of 180 MeV on the free energy available in these *p*Pb collisions, which could dissociate or inhibit the formation of charmonium states, indicating no significant in-medium dissociation of the χ_{cJ} ($J = 1, 2$) states [91].

The LHC detectors have also observed B_c^+ mesons in HICs [93]. CMS examined the production of the B_c^+ meson in Pb-Pb and *pp* collisions at $\sqrt{s_{NN}} = 5.02$ TeV through its decay channel $B_c^+ \to (J/\psi \to \mu^+\mu^-)\mu^+\nu_\mu$ [93]. The left panel of Fig. 7 presents the measured B_c^+ cross-section. The two bins of the trimuon p_T correspond to different rapidity
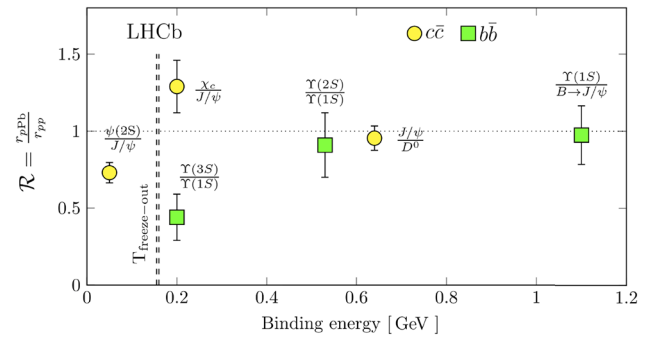

Fig. 6 (Color online) Double ratio of the quarkonium state yield relative to its ground state or open heavy quark meson in *p*Pb compared to *pp* collisions as a function of the binding energy of the quarkonium state. From Ref. [91]

ranges (see Ref. [93]). The ratio between the low p_T and high p_T regions was $18.2^{+1.3}_{-2.1}$ in *pp* data and 24.1 in the simulation, suggesting that the simulation overestimated the spectrum steepness of the spectrum [93]. The right panel of Fig. 7 shows the nuclear modification factor for the B_c^+ meson, obtained by comparing the production cross-sections in Pb-Pb to *pp* collisions measured across different transverse momentum and collision centrality bins. The B_c^+ meson showed less suppression than the quarkonia and most open heavy-flavor mesons, indicating that hot and dense nuclear matter created in HICs may enhance its production [93]. This finding provides a valuable new insight into the complex dynamics of the suppression and enhancement mechanisms of heavy quarkonia in hot dense matter. This is another connection to the study of the structure of heavy quarkonium(-like) states and HICs.

Fig. 5 (Color online) Left: Ratio of the production cross-sections for $X(3872)$ to $\psi(2S)$ in the $J/\psi\pi^+\pi^-$ decay channel, measured in various collision systems. Right: Nuclear modification factor $R_{p\text{Pb}}$ for $X(3872)$ and $\psi(2S)$ hadrons. From Ref. [90]
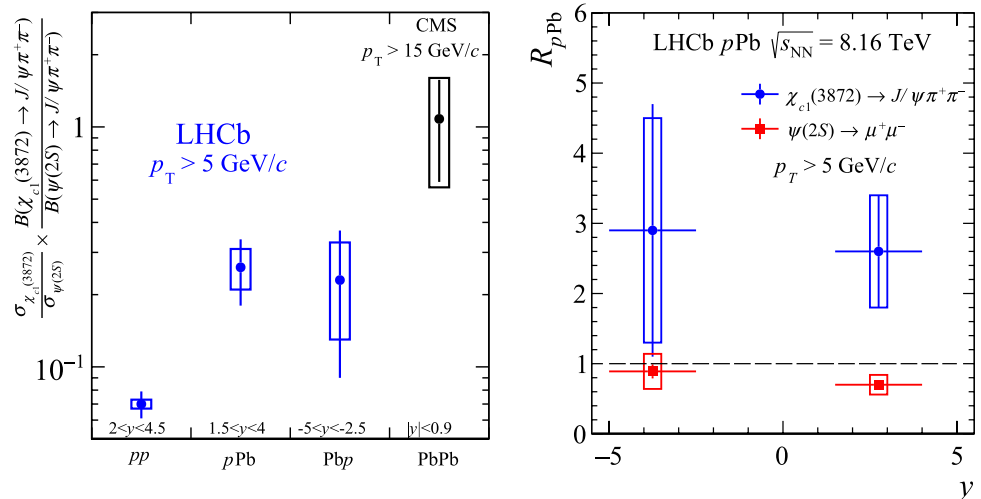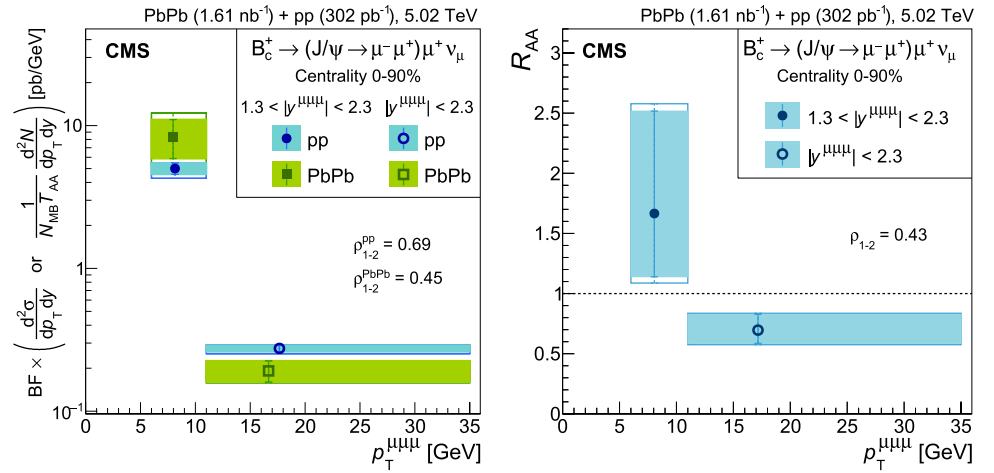
Fig. 7 (Color online) B_c^+ meson production in *pp* and Pb-Pb collisions at LHC energies. From Ref. [93]

3.2 Production in *pp*/*pp̄* collisions

3.2.1 Exotic hadrons with heavy quarks

Exotic hadrons can be produced in *pp*/*pp̄* collisions mainly in two ways: in weak decays of *b*-flavored hadrons, and in prompt processes. The former, through the $b \to c\bar{c}s$ process at the quark level, is a prominent source of exotic hadrons, with examples such as the $X(3872)$, $Z_c(4430)$ and several P_c states discussed in Sect. 2. The latter directly produces exotic hadrons through strong interactions and is the focus of this section.

Shortly after the discovery of $X(3872)$ in *B* decays by the Belle Collaboration [16], the CDF and D0 Collaborations reported the observation of $X(3872)$ in *pp̄* collisions in semi-inclusive processes [94, 95]. Subsequently, semi-inclusive production of $X(3872)$ in *pp* collisions was observed by the CMS and LHCb Collaborations [96–98]. All of these observations were made in the $J/\psi\pi^+\pi^-$ final state.

Using CDF measurements of the yields of $X(3872)$ [99] and $\psi(2S)$ [100], the prompt production rate of $X(3872)$ in *pp̄* collisions at 1.96 TeV was estimated to be [101, 102]

$$\sigma[p\bar{p} \to X(3872) + \text{all}]\text{Br}\big[X \to J/\psi\pi^+\pi^-\big]$$
$$\approx (3.1 \pm 0.7) \text{ nb,} \tag{2}$$

where the undetected particles produced in association with the $X(3872)$ are denoted by "all". Taking the branching faction of $X(3872) \to J/\psi\pi^+\pi^-$ from the RPP [22], $(3.5 \pm 0.9)\%$, we obtained the $X(3872)$ production cross-section at the CDF II detector as follows:

$$\sigma[p\bar{p} \to X(3872) + \text{all}] = (89 \pm 30) \text{ nb.} \tag{3}$$

It was proposed in Ref. [101] that such a large cross-section conflicts with the hadronic molecular picture of $X(3872)$ based on the following inequality[2]

$$\sigma(\bar{p}p \to X + \text{all})$$
$$\sim \left| \int d^3\boldsymbol{k} \langle X \mid D^0\bar{D}^{*0}(\boldsymbol{k}) \rangle \langle D^0\bar{D}^{*0}(\boldsymbol{k}) \mid \bar{p}p \rangle \right|^2$$
$$\simeq \left| \int_{\mathcal{R}} d^3\boldsymbol{k} \langle X \mid D^0\bar{D}^{*0}(\boldsymbol{k}) \rangle \langle D^0\bar{D}^{*0}(\boldsymbol{k}) \mid \bar{p}p \rangle \right|^2 \tag{4}$$
$$\leqslant \int_{\mathcal{R}} d^3\boldsymbol{k} |\Psi(\boldsymbol{k})|^2 \int_{\mathcal{R}} d^3\boldsymbol{k} \left| \langle D^0\bar{D}^{*0}(\boldsymbol{k}) \mid \bar{p}p \rangle \right|^2$$
$$\leqslant \int_{\mathcal{R}} d^3\boldsymbol{k} \left| \langle D^0\bar{D}^{*0}(\boldsymbol{k}) \mid \bar{p}p \rangle \right|^2,$$

where the undetected particles are assumed to be spectators, $\mathcal{R}$ is the region of the phase space where $X(3872)$ is produced, and $\Psi(\boldsymbol{k})$ is the wave function of $X(3872)$. It was argued in Ref. [101] that $\mathcal{R}$ should be of the order of the binding momentum of $X(3872)$, $\gamma_X \sim 35$ MeV, such that the approximate upper bound in Eq. (4) is approximately 0.1 nb, which is three orders of magnitude smaller than the measured cross-section using Eq. (3).

The estimate of $\mathcal{R}$ as the binding momentum scale has been criticized in Refs. [102–104] (see also the discussion in Ref. [7]). In Ref. [102], the authors argued that $\mathcal{R}$ should be of the order of the inverse of the force range. As an approximate estimate, the inverse of the force range is one order of magnitude larger than γ_X (see below), and the upper bound in Eq. (4) is then enlarged by a factor of $\mathcal{O}(10^3)$ compared with the estimate in Ref. [101] and agrees with the measured value from Eq. (3).

We now argue that the inverse of the force range for the $D\bar{D}^*$ *S*-wave interaction should be of the order of a few

---

[2] Although, for simplicity, we only spell out the $D^0\bar{D}^{*0}$ component, it should be understood as the proper positive *C*-parity combination of $D^0\bar{D}^{*0}$ and $\bar{D}^0D^{*0}$. The same applies to $D\bar{D}^*$.
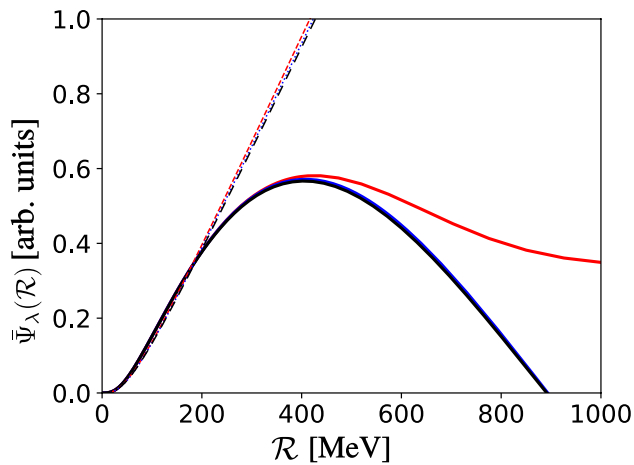
Fig. 8 (Color online) Averaged wave functions of the deuteron in the $\mathcal{R}$ region. The solid and dashed lines are the results with and without OPE, respectively, and the red, blue, and black lines correspond to the values of the cutoff $\lambda = 0.8$, 1.5, and 4.0 GeV, respectively (the blue and black curves almost overlap each other). Adapted from Ref. [104]

Fig. 9 (Color online) Illustration of the semi-inclusive production of $X(3872)$ in high-energy collisions. The circled cross presents the source for $X(3872)$ and its associated particles in the production, denoted as "all". (a) presents the $D\bar{D}^*$ loop contribution, and (b) represents a counter term required to absorb the UV divergence from the loop

hundred MeV. However, because the *u*-channel one-pion exchange (OPE) between D and D^* has a scale of $\mu_\pi = \sqrt{\left(M_{D^{*0}} - M_{D^0}\right)^2 - M_{\pi^0}^2} \approx 44$ MeV, the main binding force for $X(3872)$ is probably not the OPE assumed in Ref. [30]. First, the renormalization of the OPE potential requires short-distance counter terms (see, for example, Ref. [105]). Second, phenomenological studies suggest the importance of light vector-meson exchanges (see, for example, Refs. [106–109]). Third, the binding energies of the hidden-charm hadronic molecules predicted in Ref. [110] change only marginally when the OPE is included, compared to the case with only constant contact terms. Fourth, by analyzing the contributions from different Wick contractions in the lattice QCD calculation of the isoscalar DD^* interaction directly related to $T_{cc}(3875)^+$, Ref. [111] reported that the ρ exchange may be crucial for inducing the attraction between DD^*, in line with phenomenological studies [112, 113]. It is reasonable to assume that the $D\bar{D}^*$ system experiences a similar situation, which may be tested using lattice QCD calculations.

To demonstrate that the choice of $\mathcal{R} \simeq \gamma_X$ is too small, in Ref. [104], the authors considered deuterons as an example. The binding energy of the deuteron is approximately 2.2 MeV, and the binding momentum is $\gamma_d \simeq 45$ MeV. Figure 8 shows the averaged wave functions of the deuteron in the $\mathcal{R}$ region [104], $\bar{\Psi}_\lambda(\mathcal{R}) \equiv \int_{\mathcal{R}} \mathrm{d}^3 k \Psi_\lambda(k)$, where λ is the regulator introduced to render the wave function well defined (for details, see Ref. [114]). It is clear that the wave function is far from saturated in the region $\lesssim \gamma_X$, and saturation is achieved only when $\mathcal{R}$ is a few hundred MeV, in line with the argument in Ref. [102].
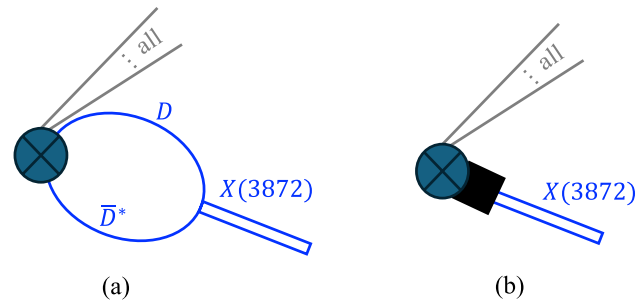
This can be understood by considering the diagram corresponding to the second line of Eq. (4), as shown in Fig. 9 (a).[3] Because the charmed meson pair is produced during high-energy collisions with all the particles produced in association with $X(3872)$ assumed to be spectators, the production of $D\bar{D}^*$ occurs over short distances as a point-like vertex. The loop integral shown in Fig. 9a is ultraviolet (UV) divergent and can be regularized using a cutoff. A cutoff-dependent counter term is required to absorb the divergence, as shown in Fig. 9b, to render the full-amplitude cutoff independent. For the counter term to be of natural size, that is, of the same order as the loop, the cutoff should also take a natural value for a hard scale, which is again of the order of the inverse of the force range, that is, a few hundred MeV.

The static properties of $X(3872)$, such as the mass and J^{PC} quantum numbers, can be understood through the $D\bar{D}^*$ hadronic molecular component. However, this does not mean that all properties are predominantly determined by the long-distance $D\bar{D}^*$ component. The production of $X(3872)$ in high-energy collisions is a dynamic process, and the mechanism involved is generally different from that responsible for the internal structure. It involves the production of a pair of charm and anti-charm quarks at short distances, the hadronization of these quarks into charm and anti-charm mesons at intermediate distances ($\sim 1/\Lambda_{QCD}$), and the coalescence of these charm mesons into $X(3872)$ at long distances ($\sim 1/\gamma_X$) (for a discussion on the factorization of long- and short-distance factors for the production and decay of $X(3872)$, see Ref. [115]). The counter term in Fig. 9b refers to the short-distance production of $X(3872)$ from sources other than the $D\bar{D}^*$ intermediate state with low relative momenta and includes contributions from, for example, the production of $X(3872)$ from a $c\bar{c}$ pair through hadronization. The prompt

---

[3] Here, the charmed meson pair can be both the neutral $D^0 \bar{D}^{*0}$ and charged $D^+ D^{*-}$.

production of $X(3872)$ from $c\bar{c}$ operators in high-energy hadronic reactions can be studied using a nonrelativistic QCD framework, as discussed in Refs. [102, 116–118].

Another method to make the entire production amplitude cutoff independent is to consider the factorization formula, as discussed in Ref. [115]. The production of $X(3872)$, or more generally, hadronic molecules, contains both long-distance and short-distance parts. The long-distance part has a typical momentum scale of the $X(3872)$ binding momentum and is given by the coupling of $X(3872)$ to $D\bar{D}^*$, which is fixed from the binding momentum for a pure composite system [7, 119] or equivalently expressed in terms of the universal wave function for S-wave loosely bound states [102, 120]. The momentum scales in the short-distance part are of the order of the inverse of the force range or larger. The loop integral shown in Fig. 9a regularized using a hard three-momentum cutoff is $G_\Lambda \propto 2\Lambda/\pi + ik$, where k is the magnitude of D or $\bar{D}^*$ in the $D\bar{D}^*$ c.m. frame. For Λ of the order of the inverse of the force range, the first terms are dominant. The Λ-dependence of the loop can be absorbed by the production vertex of $D\bar{D}^*$ from high-energy collisions, $P_\Lambda \propto 1/\Lambda$, and the short-distance part of the production amplitude is given by the product $P_\Lambda G_\Lambda$.

In Refs. [104, 121], the authors performed order-of-magnitude estimates of the cross-sections for prompt production in $pp/p\bar{p}$ collisions of $X(3872)$ as a $D\bar{D}^*$ hadronic molecule. The $D\bar{D}^*$ cross-sections were estimated using the Monte Carlo event generators Pythia and Herwig following Refs. [101–103]. The $D\bar{D}^*$ loop shown in Fig. 9a was regularized using a Gaussian form factor with a cutoff $\in [0.5, 1.0]\,\text{GeV}$, corresponding to $\mathcal{R} \in [0.3, 0.6]\,\text{GeV}$ [104]. Correspondingly, the estimated cross-section for the production of $X(3872)$ in $p\bar{p}$ collisions with CDF kinematics was $\sim [7(5), 29(20)]$ nb [104], where the values outside (inside) the parentheses were obtained using Herwig (Pythia). This estimate agrees with the measured value from Eq. (3) at the order-of-magnitude level. The estimate for production in pp collisions at 7 TeV is approximately $\sim [13(4), 55(15)]$ nb [104], which is in agreement with (30 ± 9) nb[4] measured by the CMS Collaboration [97].

$X(3872)$ is a hidden-flavor exotic hadron, the dominant component of its wave function for describing its static properties is not necessarily its lowest Fock space components ($q\bar{q}$ with $q = u, d, s, c$). In this case, a small $c\bar{c}$ component

---

[4] This was obtained using

$$\sigma[pp \to X(3872) + \text{all}]\,\text{Br}\left[X \to J/\psi\pi^+\pi^-\right]$$
$$\approx (1.06 \pm 0.11 \pm 0.15)\ \text{nb},$$

measured by the CMS in the kinematic region $10 < p_\text{T} < 30$ GeV and $|y| < 1.2$, where p_T and y are the transverse momentum and rapidity of $X(3872)$, respectively, [97].

may be the driving force to produce $X(3872)$ in high-energy collisions, even if $X(3872)$ is predominantly molecular. Consequently, for a high-energy collision at a squared c.m. energy of s, the scaling (in powers of s) of the differential cross-section should follow the constituent counting rule [122] for the $c\bar{c}$ component, despite its main component still having four constituent (anti)quarks (see also Ref. [123]). This contrasts with the deuterons and other light (hyper) nuclei discussed in Sect. 3.1, whose lowest Fock space component has $3A$ quarks, where A is the number of baryons inside the (hyper)nuclei. Therefore, it is natural that the $X(3872)$ production cross-section at large p_T is orders of magnitude larger than those of the deuteron and other light (hyper)nuclei measured by ALICE [68, 124]. Moreover, the critique in Ref. [125] on the molecular picture of $X(3872)$ based on a large difference does not hold true.

With the same reasoning, because $f_0(980)$ is also a hidden-flavor meson, the lack of observation of an enhancement of the p_T-differential $f_0(980)/K^*(892)^0$ ratio in pPb collisions by ALICE [126] should not be regarded as evidence for the $f_0(980)$ being a normal $q\bar{q}$ meson or against the $K\bar{K}$ hadronic molecular picture [127, 128]. Similarly, the scaling of the elliptic anisotropic flow parameter v_2 for the production of $f_0(980)$ in pPb collisions at the CMS experiment [129] likely agrees with a two-constituent hypothesis and should not be regarded as evidence for $f_0(980)$ being a normal $q\bar{q}$ meson.

As discussed in Sect. 3.1, the LHCb measured the production of $X(3872)$ and $\psi(2S)$ as functions of the charged-particle multiplicity in pp collisions at 8 TeV [98]. The measured ratio of the yields of $X(3872)$ to $\psi(2S)$ in the $J/\psi\pi^+\pi^-$ decay channel decreased as the charged-particle multiplicity increased. This behavior is in line with the result obtained in the comover interaction model, assuming the diameter of $X(3872)$ (as a compact tetraquark) to be 1.3 fm, and differs drastically from the hadronic molecular picture of $X(3872)$ obtained with a coalescence model [130]. This conclusion was challenged in Ref. [131]. In Ref. [130], the cross-section for breaking up $X(3872)$ as a hadronic molecule by scattering with comoving particles was assumed to be inversely proportional to the $X(3872)$ binding energy. However, in Ref. [131], the authors argued that the breakup cross-section can be approximated by the probability-weighted sum of the cross-sections for the scattering of comoving pions with constituent charmed mesons inside $X(3872)$. This is because for $X(3872)$ with such a small binding momentum γ_X, the comoving particles can easily probe the internal structure of $X(3872)$ and thus scatter directly with the constituent particles. Consequently, the breakup cross-section should be insensitive to the $X(3872)$ binding energy. By modifying the comover interaction model, the LHCb data can be described well under the hadronic molecular picture of $X(3872)$, as shown in Fig. 10 [131].
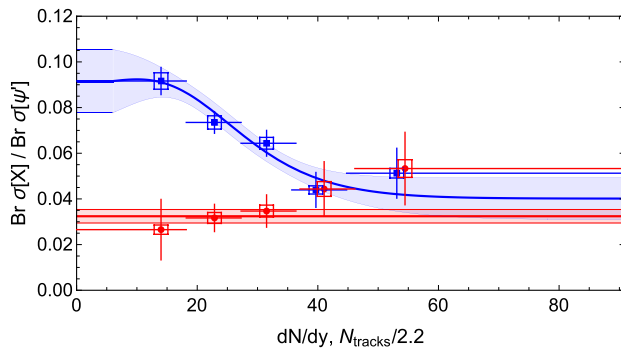
Fig. 10 (Color online) Ratios of the *X*(3872) and *ψ*(2*S*) cross-sections (blue: from prompt productions; red: from *b*-hadron decays) measured in the $J/\psi\pi^+\pi^-$ channel as functions of the multiplicity d*N*/d*y*. The data were measured by LHCb [98], and the curves with uncertainty bands were obtained from fitting to the LHCb data in Ref. [131]. From Ref. [131]

3.2.2 Light-flavor hadron production

In previous discussions, exotic hadronic states such as charm and beauty quarks were primarily examined within systems featuring heavy-flavor quarks. There are also many hadronic states in the light-flavor sector with properties that do not align with traditional quark model predictions. For example, the mass of $\Lambda(1405)$ is lower than that of non-strange $N(1535)$ with the same J^P quantum numbers, even though $\Lambda(1405)$ contains a heavier *s* quark from the perspective of the three-quark baryon model. In the 1950 s, $\Lambda(1405)$ was predicted as a bound state of $K\bar{N}$ by Dalit and Tuan [132] before its discovery. Since the 1990 s, $\Lambda(1405)$ has been considered as a molecular state of $K\bar{N}$ [133], accompanied by another nearby pole in the coupled-channel ($\pi\Sigma$-$\bar{K}N$) scattering amplitudes, known as the two-pole structure for $\Lambda(1405)$ [134]. The second and lower poles are now listed as $\Lambda(1380)$ in the latest version of the RPP [22]. Similarly, in a light-meson system, the lowest scalar octet is considered a ground state family of tetraquarks [135], and $f_0(980)$ is a good candidate for the $K\bar{K}$ molecule [127, 128].

It is also important to investigate the possible dibaryon states to better understand baryon interactions beyond protons and neutrons. To date, the only well-established dibaryon molecular state is the deuteron state, whereas the internal structure of another candidate, $d^*(2380)$ [136],

discovered over a decade ago, remains unclear. A common explanation for this is that $d^*(2380)$ is a double $-\Delta$ state [137–139]. A resonance peak was recently observed below the threshold in the $\bar{K}NN$ system, with preliminary studies indicating ΛN is the main decay channel [140].

In low-to-moderate energy *pp* and *p* $\bar{p}$ collisions, specifically with c.m. energies below 3.5 GeV and especially near the thresholds of certain rare decay channels, exclusive measurements can provide detailed information on many reactions, facilitating sophisticated theoretical modeling. There are large experimental data samples for *pp* and *p* $\bar{p}$ collisions in this energy region, for example, the IUCF, HADES, CELSIUS, and COSY experiments (for reviews, see Refs. [141, 142]). Here, we illustrate how the study of final-state systems in few-body reactions from *pp* and *p* $\bar{p}$ collisions can be used to search for baryon excited states, dibaryons, and meson excited states and discuss how to identify more exotic states and study their properties. There are three types of tree diagrams, as shown in Fig. 11, where (a), (b), and (c) indicate the main mechanisms for searching for the baryon excited states, dibaryons, and meson excited states, respectively.

The search for baryon excited states relies primarily on different final state combinations. By applying selection rules based on isospin conservation, regions with significant contributions from certain particles can be identified for further study. For example, in the $pp \to pn\pi^+$ process, although $N(1440)N\sigma$ has a significant impact [143], the largest contribution originates from $\Delta(1232)^{++} \to p\pi^+$, making peaks such as $N(1440)$ less prominent. Conversely, in $\bar{p}p \to \bar{p}n\pi^+$, the contribution of $\Delta(1232)^{++}$ is absent, and the cross-section for other charged $\Delta(1232)$ states decreases by a factor of nine because of the isospin factor, leading to increased visibility of peaks such as $N(1440)$ [144]. Another example is in the $pp \to n\Sigma^+K^+$ process [145, 146], where Σ^+K^+ can only form isospin-3/2 states, thus providing a good venue for detecting Δ baryon excited states. In previous experiments, measurements were performed for many final states, such as $pp \to pp\pi$, $pp\eta$, $pp\phi$, $pK+\Sigma^0$, and $pK+\Lambda$. It is important to consider the interaction between the initial and final states by using various methods to handle the final state interaction [141]. Despite the complexity of these theoretical methods, they can only explain a portion of experimental data. For example, in $pp \to pp\eta$, only data for the c.m. energy of 12 MeV above the $pp\eta$ threshold

Fig. 11 Illustration of the tree diagrams of the *NN* reaction to few-body final states, where the solid lines represent nucleons, dashed lines represent mesons, and double lines represent baryon and dibaryon resonances

(*a*)   (*b*)   (*c*)
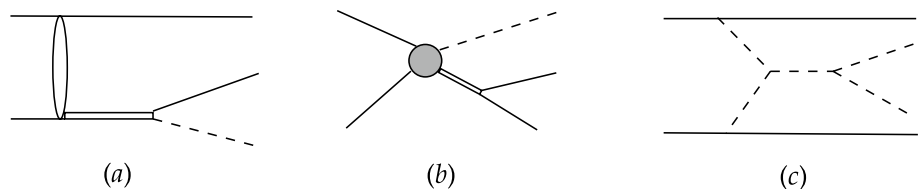
can be well described, whereas the double-peak structure in the $p\eta$ invariant mass spectrum at higher energies cannot be explained by considering only known excited nucleons [147]. Furthermore, polarization data cannot be explained by existing models [141]. Another issue is that because of this complication, only a single reaction process is typically analyzed, such as the analysis of $pp \to pK\Lambda$ in Ref. [148]. However, when considering the $K\Lambda$ resonance states, although the threshold starts from approximately 1.6 GeV, which covers the $N(1650)$ region, $N(1535)$ could also make a significant contribution, owing to the presence of hidden strangeness in this state [149]. A better approach involves a combined analysis of multiple final states to extract information on multiple resonances. Similarly, the hidden-charm P_c states in $pp(\bar{p}) \to pp(\bar{p})J/\psi$ and $pp(\bar{p}) \to pp(\bar{p})\eta_c$ reactions may be investigated [150].

pp and pd collisions offer good locations to search for dibaryon states. In reactions with either single-pion or double-pion production or with $K\Lambda/K\Sigma$ in the final states, apart from the threshold cusp effect in $K\Sigma$, no dibaryon states were observed [151] until 2014 when the Wide Angle Shower Apparatus (WASA) experiment at the Cooler Synchrotron (COSY) established a narrow resonant structure d^* in the $pn \to NN\pi\pi$ reaction, with $I(J^P) = 0(3^+)$ and a width of 70 MeV [136]. It was proposed to be a double-Δ molecular state [137–139], although whether this corresponds to a genuine resonance is still under debate [152]. For theoretical predictions prior to the experimental observations, we refer to the review [151]. In particular, the quark model prediction for an isospin-3/2 dibaryon in Refs. [153, 154] agreed well with the measured mass. In theory, a notable feature of $d^*(2380)$ is that its width is considerably smaller than that of two Δ baryons, implying the possible presence of many compact six-quark components in $d^*(2380)$ [151, 155], although there is still no definitive conclusion. This discovery opens up a new direction in the search for dibaryon states. For pp reactions, as shown in Fig. 11b, new dibaryon states may be formed by emitting one or more mesons. Recently, in the J-PARC E15 experiment [140], a resonance peak structure with a width of 100 MeV was found in the $\Lambda + p$ final state in the reaction $K^- + {}^3\text{He} \to (K^- + pp) + n \to (\Lambda + p) + n$ below the threshold of $\bar{K}NN$ by approximately 40 MeV, indicating the existence of a ΛN dibaryon state. The existence of this resonance peak can be verified in the $pp \to K\Lambda p$ reaction; however, the energy at the COSY is only at the threshold for producing this peak structure [156]. Previous theoretical calculations for this reaction that did not consider the influence of the peak structure must be revised [157]. For further discussion on the production of dibaryon states in pp collisions, refer to [158–160].

To produce excited meson states in the low-energy region, the contribution presented in the diagram in Fig. 11c in exchanging two particles is expected to be smaller than that in the other two diagrams. However, in the high-energy region, the intermediate exchanged meson can be replaced by a pomeron, and the fusion of the two exchanged pomerons to produce mesons plays a crucial role in producing double-pion and double-kaon resonant particles through diffraction processes [161, 162]. Owing to its gluon-rich environment, this reaction is often used to search for another type of exotic state, that is, glueballs, in high-energy pp or $p\bar{p}$ reactions. For calculations of the production of $PC = ++$ mesons, such as $f_0(980)$, $f_2(1270)$, and $f_0(1500)$, considering the pomeron-pomeron fusion, we refer to Refs. [163–165].

Finally, note that considering only the tree diagram mechanisms in Fig. 11 to estimate the production of light hadrons in pp collisions offers a rough approximation. The loop contributions in hadronic reactions are often crucial. For reactions with multiple hadrons in the final state, the final-state interactions and coupled-channel effects may be crucial and can significantly affect the extraction of resonance properties. Therefore, it is essential to use comprehensive coupled-channel models for few-body systems and a combined analysis of various related reactions to extract the resonance poles. Relevant efforts have been made in, for example, the Jülich-Bonn model [166], Argonne-Osaka model [167], and three-body unitary models [168, 169]. However, such models must include many parameters, and obtaining convincingly determined model parameters requires a significant amount of experimental input. Therefore, additional experimental data are required.

3.3 Production in heavy-ion collisions

In this subsection, we briefly review recent studies on the production of $X(3872)$ and T_{cc}^+ in HICs. Earlier reviews on related topics can be found in Refs. [15, 170–172].

As discussed in Sect. 3.1, the only reported signal of prompt $X(3872)$ production in HICs originated from the CMS collaboration [85]. The yields, evolution, and distributions of $X(3872)$ as well as those of other exotic hadrons produced in HICs are complicated by the surrounding QCD medium/nuclear matter/pion gas.

Various coalescence models [73, 173–175] and statistical hadronization models (SHMs) [176] have been used to estimate the yields of $X(3872)$ in hadronic molecular and compact tetraquark pictures. The former depend on a suitable wave function in the coordinate space to encode structural information (for discussions on the subtlety of the short-distance part, see Sect. 3.2.1). In the instantaneous coalescence model, there are still several unclear parameters, such as the volume size at which coalescence occurs, available light quark number at the hadronization temperature, and oscillator frequency of the Wigner function. The SHM assumes that hadrons are in thermal and chemical equilibrium, that is, with a charm-quark fugacity factor to ensure charm-quark
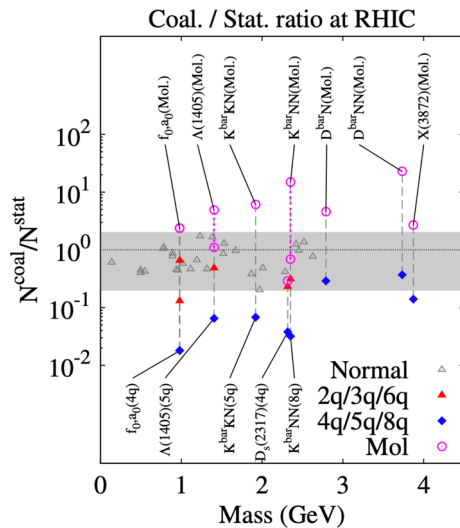
Fig. 12 Ratios between the yields in the coalescence and statistical models [73]. The gray band is the region for normal hadrons. From Ref. [73]
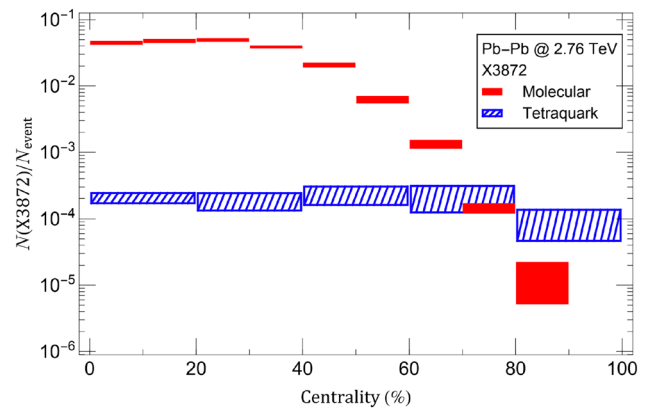

Fig. 13 (Color online) Centrality dependence of $X(3872)$ in Pb-Pb collisions at $\sqrt{s_{NN}} = 2.76$ TeV in both the molecular (red solid boxes) and compact tetraquark (blue shaded boxes) pictures obtained in Ref. [175]. The uncertainties are purely statistical. From Ref. [175]

conservation. The yield of $X(3872)$ in this model depends only on its mass and not on its internal structure.

In Ref. [73], the authors used both coalescence and statistical models to estimate the yields of various hadrons at the RHIC, and the model results are summarized in Fig. 12. As shown in the figure, compared to the yield of normal hadrons, that of a compact tetraquark is typically one order of magnitude smaller, and that of a hadronic molecule is a factor of two or more. However, the coalescence model considered does not include the evolution effect in the medium, and the statistical model depends only on the masses of the hadrons instead of their internal structures.

Further information to deepen our understanding of the nature of exotic hadrons includes information on their various distributions, such as, the centrality, rapidity, and transverse momentum distributions. As reported in Ref. [175], a multiphase transport model was used to estimate the yield of $X(3872)$ in Pb-Pb collisions at $\sqrt{s_{NN}} = 2.76$ TeV. Considering that the fireball volume is crucial in the production of $X(3872)$, they concluded that the yield of $X(3872)$ in the molecular picture was two orders of magnitude larger than that in the compact picture, and significant centrality dependence was obtained (see Fig. 13). In addition, the corresponding rapidity and transverse momentum spectra, as well as the elliptical flow coefficient v_2 versus the transverse momentum for $X(3872)$ in the molecular picture, were also predicted. The same method was used to estimate the production of the double-charm tetraquark state T_{cc}^+ [177] in Pb-Pb collisions at $\sqrt{s_{NN}} = 2.76$ TeV in the molecular picture. The ratio between the yields of T_{cc}^+ and $X(3872)$ decreased with centrality, which agrees with the

experimental fact that the yield of T_{cc}^+ is approximately two orders of magnitude smaller than that of $X(3872)$.

When the wave function among the constituents is considered, for example, the Wigner function described in Ref. [178], the coalescence probability decreases owing to the strict constraints on the relative momentum between constituents, despite the large geometric size of hadronic molecules [178]. In this case, Ref. [178] showed that the total yield of a compact tetraquark $X(3872)$ is several times larger than that of the molecular picture for Pb-Pb collisions. Simultaneously, the effect of fireball volume on centrality dependence in the molecular picture is not as significant as that described in Ref. [175]. In addition to the distribution of $X(3872)$, the evolution of charm quarks in QGP was also explored in Ref. [178] using the Langevin equation. The yields in both scenarios decreased with evolution time. The same method has been applied to a double-charm tetraquark state [179].

There was also an early study [180] based on the SU(4) effective Lagrangians that considered the evolution of $X(3872)$ by calculating the corresponding production and absorption cross-sections to estimate the hadronic effects on the $X(3872)$ meson abundance in HICs. The absorption cross-sections of the $X(3872)$ meson by pions and ρ mesons during the hadronic stage of HICs were evaluated. They estimated the yield of $X(3872)$ in HICs using both the statistical and coalescence models. They found that the absorption cross-section was two orders of magnitude larger than the production cross-section, and the time evolution of $X(3872)$ abundance in the HICs was stable (see Fig. 14), which is in contrast to the conclusions of Ref. [178].

The production of $X(3872)$ in HICs is due to a large number of heavy quarks, as many as 20 $c\bar{c}$ pairs per unit rapidity, in Pb-Pb collisions at LHC energies [73, 181]. Charm quarks are free to move through large volumes and can coalesce to
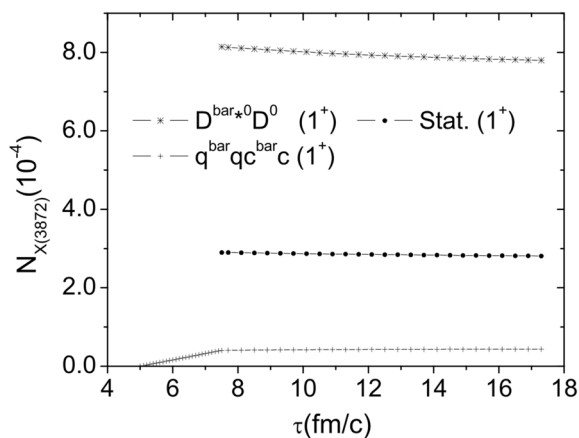
Fig. 14 Time evolution of $X(3872)$ in the hadronic molecular and compact tetraquark pictures in central Au-Au collisions at $\sqrt{s_{NN}} = 200$ GeV with quantum number $J^P = 1^+$ from the calculations in Ref. [180]. From Ref. [180]

form bound states at the end of the QGP phase or their mixtures. A thermally averaged cross-section was proposed in Refs. [181, 182], with the dissociation and production processes estimated using $X + \pi \to \bar{D} + D$, $X + \pi \to \bar{D}^* + D^*$, $D + \bar{D} \to X + \pi$ and $\bar{D}^* + D^* \to \pi + X$, respectively. Because these studies were based on the coalescence model, their conclusions were similar. That is, the cross-sections in the molecular picture were larger than those in the compact tetraquark picture [181, 182], owing to geometrical arguments [181]. The detailed numbers were scheme-dependent. However, the geometrical estimate of cross-sections cannot be used in high-energy collisions because the particles that scatter with $X(3872)$ can have sufficient momentum to probe into $X(3872)$ and thus the size of $X(3872)$ is no longer important [131]. The same method was also applied to the double-charm tetraquark T_{cc}^+ in both the LHC and RHIC energy regions within both the molecular and compact tetraquark pictures [183].

In Ref. [184], a transport calculation of $X(3872)$ through the fireball formed during Pb-Pb collisions at $\sqrt{s_{NN}} = 5$ TeV was reported. The formation and dissociation of $X(3872)$ depend on two transport parameters: its inelastic reaction rate and thermal equilibrium limit in an evolving hot QCD medium. The latter was controlled by the charm production cross-section in primordial nucleon-nucleon collisions. They found that the yield of the loosely bound molecule, assumed to have formed later in the fireball evolution than in the tetraquark, was a factor of two smaller than that of the compact tetraquark. The same bulk-medium evolution used for charmonium and bottomonium transport was implemented, which was approximated by a cylindrically expanding fireball volume with a transverse flow profile of the blast-wave type. They used evolution parameters that reproduced the fits to empirical light-hadron spectra (pions, kaons, and protons)

at thermal freeze-out temperatures. This resulted in the relative yields for the hadronic molecule and compact tetraquark pictures in Ref. [184] being qualitatively different from most coalescence model calculations [73, 173–175]. In Ref. [184], the initial hadronic abundance of the molecular configuration was assumed to be zero, which is different from the instantaneous coalescence models described in Refs. [73, 175], where the assumption of a wave function provides a large phase space and results in a significant surpassing of the equilibrium limit. The difference in these results may be regarded as a showcase of the model dependence for estimating the production of exotic hadrons in HICs, owing to the complications of the QCD medium.

In Ref. [185], the authors studied the properties of $X(3872)$ in a hot-pion bath based on its molecular picture. They found that its width became a few tens of MeV at temperatures of $100 - 150$ MeV and its normal mass moved above the DD^* threshold. Their calculation was based on the SU(4) effective Lagrangians and imaginary time formalism in a self-consistent approach. The peak associated with $X(3872)$ became significantly wider with increasing temperature. This is because of the appearance of a finite imaginary part of the amplitude at the pole position when temperature effects were included. Their results indicated that at typical kinetic freeze-out temperatures at the RHIC and LHC, $X(3872)$ cannot be considered a loosely bound state. In contrast, a compact tetraquark-type state, which should couple weakly to $D\bar{D}^*$ because otherwise, a large molecular component is unavoidable, would barely change its behavior under the same circumstances.

Recently, a more rigorous treatment of the thermal corrections from the hot pion gas to the propagator of a loosely bound charm-meson molecule was presented using a zero-range effective field theory (ZREFT) [186]. One might simply expect that ZREFT cannot be applied at a high temperature, which is characterized by the kinetic freeze-out temperature and is orders of magnitude larger than the binding energy of a loosely bound state. Fortunately, the authors of Ref. [186] illustrated that ZREFT can be applied to such a system by first integrating out thermal pions, leaving the ZREFT parameters temperature-dependent. The only correction to the binding energy is a small temperature-dependent correction to the complex binding momentum. It is noticed that the thermal corrections to the binding energy of the molecule only appear at the next-to-leading order, and the results are shown by Fig. 15. These results indicate that loosely bound molecules, such as $X(3872)$ and T_{cc}^+, can survive in the thermal environment of a hadron gas at sufficiently low temperatures. This conclusion is consistent with the large rate of $X(3872)$ production in Pb-Pb collisions obtained by the CMS Collaboration.

Very recently, in Ref. [187], the authors proposed that the production rate of a loosely bound hadronic molecule, such as $X(3872)$, in HICs can be expressed in terms of the

Fig. 15 (Color online) Real parts of the poles of two-body propagators (left-panel) and the thermal widths (right panel) for $X(3872)$ (red solid curves), and T_{cc}^+ (blue solid curves) in the pion gas as a function of temperature T [186]. The dashed lines in the left panel are the thresholds of the constituent charm-meson pair, and those in the right panel are the sum of the decay widths of the constituents. From Ref. [186]
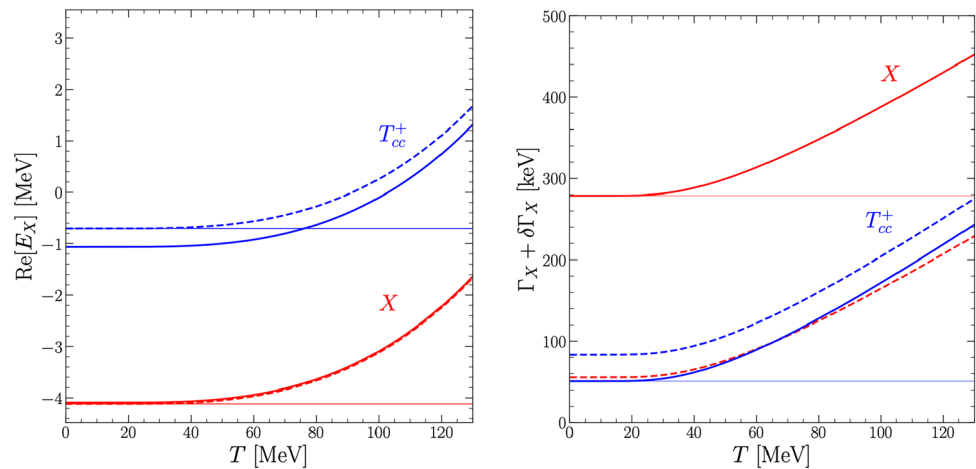
short-distance contact density at the kinetic freeze-out of the hadron gas, which approaches a nonvanishing limit as the binding energy decreases to 0.

Because both $X(3872)$ and $\psi(2S)$ can be reconstructed in the $J/\psi\pi^+\pi^-$ channel, the production of $X(3872)$ is often compared to that of $\psi(2S)$ (see, for example, Fig. 5). For instance, the prompt $X(3872)$ to $\psi(2S)$ yield ratio was found to be [85]

$$\mathcal{R} = \frac{N_{X(3872)}}{N_{\psi(2S)}} = 1.08 \pm 0.49 \text{(stat.)} \pm 0.52 \text{(syst.)}, \qquad (5)$$

with a central value approximately one order of magnitude higher than the 0.09 observed for *pp* collisions [98]. In Ref. [188], the authors used a method similar to that in Refs. [181, 182] to estimate the thermally averaged cross-sections for the production and absorption of $\psi(2S)$ and used them in the rate equation to determine the time evolution of $N_{\psi(2S)}$. The yield ratio $N_X/N_{\psi(2S)}$ was predicted as a function of the centrality of the c.m. energy and charged hadron multiplicity measured in the mid-rapidity region $[dN_{ch}/d\eta(\eta < 0.5)]$.

Similarly, Ref. [189] presents a phenomenological model for the partonic medium attenuation effects on $X(3872)$ and $\psi(2S)$ production in both *pp* and Pb-Pb collisions. A medium-assisted enhancement effect was proposed for $X(3872)$ production, which was argued to be dominant at high parton densities and large medium sizes. Its competition with the absorption-induced suppression leads to a specific pattern of the $N_X/N_{\psi(2S)}$ ratio, which first decreases and then increases when the partonic medium evolves from a small to a large colliding system. A comparison of the results obtained in Ref. [189] with the data [85, 98, 190] is shown in Fig. 16.

In addition to the measurements of the centrality, transverse momentum, and rapidity distributions of exotic hadrons discussed in the previous subsection, an additional important observable that has recently received intensive
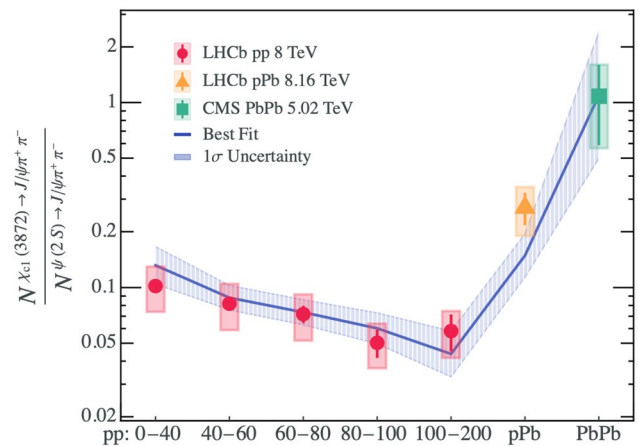
Fig. 16 (Color online) Yield of $X(3872)$ relative to that of $\psi(2S)$ obtained in Ref. [189] in comparison with the LHCb *pp* collisions data at $\sqrt{s_{NN}} = 8$ TeV (red circle) [98], LHCb *p*Pb collisions data at $\sqrt{s_{NN}} = 8.16$ TeV (orange triangle) [190], and CMS Pb-Pb collisions data at $\sqrt{s_{NN}} = 5.02$ TeV (green box) [85]. From Ref. [189]

interest is the momentum correlation between two hadrons. Because the correlation function contains information about the hadron-hadron final state interaction, exotic hadrons that couple to these two hadrons can be studied.

The momentum correlation function can be expressed in terms of the single-particle emission function $S(x_i, \boldsymbol{p}_i)$, which describes the probability of emitting a particle in space-time x_i with momentum $\boldsymbol{p}_i$ through convolution with the squared relative two-particle wave function:

$$C(\boldsymbol{q}, \boldsymbol{P}) = \frac{\int d^4x_1 d^4x_2 S_1(x_1, \boldsymbol{p}_1) S_2(x_2, \boldsymbol{p}_2) \left|\varphi^{(-)}(\boldsymbol{r}, \boldsymbol{q})\right|^2}{\int d^4x_1 S_1(x_1, \boldsymbol{p}_1) \int d^4x_2 S_2(x_2, \boldsymbol{p}_2)}.$$

The relative wave function $\left|\varphi^{(-)}(\boldsymbol{r}, \boldsymbol{q})\right|^2$ is for the hadron pair in the outgoing state that contains information about the hadron-hadron interaction. If the two hadrons are completely independent of each other, the momentum correlation

function should be equal to unity. The correlation function is often approximated as follows (see, for example, Ref. [191])

$$C(\boldsymbol{q}, \boldsymbol{P}) = \int d^3 r S_{12}(\boldsymbol{r}) \left| \varphi^{(-)}(\boldsymbol{q}, \boldsymbol{r}) \right|^2. \tag{6}$$

Typically, a spherical Gaussian source function with a given source radius is assumed, which ignores the dynamic properties of the particle emission sources. Low-energy scattering observables for various systems, including scattering lengths and effective ranges, have been extracted using this method. Many studies have been conducted along this direction, for example Refs. [170–172, 192]. For a recent review, see Ref. [15]. However, note that the results of the hadron-hadron interactions extracted using this method depend on the assumption of the source profile and source size. Although low-energy scattering observables correspond to long-distance physics, their source profile is short. On the one hand, the source function serves as a UV regulator (a form factor) for the production of the hadron pair, and the source size acts as a cutoff in the form factor. However, the correlation function measured in the experiments as physical observables should not depend on the UV regulator. From this perspective, work still needs to be performed to obtain the hadron-hadron interactions in a model-independent manner. It is worth noting that recent studies by ALICE [193, 194], which modeled the source considering a Gaussian profile and an exponential tail owing to strongly decayed resonances, suggested a common source for the meson-meson and meson-baryon sectors in *pp* collisions at the LHC.

4 Summary and outlook

Exotic hadrons remain a vibrant area of research, with significant contributions from various experiments, including Belle, BaBar, BESIII, LHC experiments, and RHIC. These experiments provide a broad and detailed understanding of exotic states, pushing the boundaries of our knowledge of QCD and its strong interactions. Herein, we present a concise review of the studies on exotic hadrons in $pp/p\bar{p}$ and nuclear collisions. An increasing amount of data is being collected on prompt production during such collisions. However, from the discussion above, it is clear that more effort is still needed to understand the production mechanisms of exotic hadrons and to shed light on their nature.

Finally, let us mention that the structure of exotic hadrons must be understood using a combination of different reactions that provide supplementary information. In addition to the nuclear collisions reviewed here, e^+e^- collisions, *b*-flavored hadron decays, and photoproduction also play unique roles in the study of exotic hadrons. For example, $X(3872)\gamma$ [195] and $Z_c(3900)$ [43, 44] were observed in e^+e^-

collisions only within a specific range of energies around the mass of $\psi(4230)$. This feature suggests that the production mechanism for these states is due to charmed-meson intermediate states that couple strongly to these exotic particles, thus providing invaluable input for understanding them.

Future upgrades to currently running experiments and ongoing research using various reactions promise further discoveries and insights into the nature of exotic hadrons.

References

1. M. Gell-Mann, A schematic model of baryons and mesons. Phys. Lett. **8**, 214–215 (1964). https://doi.org/10.1016/S0031-9163(64)92001-3
2. G. Zweig, An SU(3) model for strong interaction symmetry and its breaking. Version 2. 2–101 (1964). https://doi.org/10.17181/CERN-TH-412
3. S. Godfrey, N. Isgur, Mesons in a relativized quark model with chromodynamics. Phys. Rev. D **32**, 189–231 (1985). https://doi.org/10.1103/PhysRevD.32.189
4. S. Capstick, N. Isgur, Baryons in a relativized quark model with chromodynamics. Phys. Rev. D **34**, 2809–2835 (1986). https://doi.org/10.1103/physrevd.34.2809
5. L.Y. Glozman, D.O. Riska, The Spectrum of the nucleons and the strange hyperons and chiral dynamics. Phys. Rep. **268**, 263–303 (1996). https://doi.org/10.1016/0370-1573(95)00062-3
6. A. Esposito, A. Pilloni, A.D. Polosa, Multiquark resonances. Phys. Rep. **668**, 1–97 (2017). https://doi.org/10.1016/j.physrep.2016.11.002
7. F.K. Guo, C. Hanhart, U.G. Meißner et al., Hadronic molecules. Rev. Mod. Phys. **90**, 015004 (2018). https://doi.org/10.1103/RevModPhys.90.015004
8. S.L. Olsen, T. Skwarnicki, D. Zieminska, Nonstandard heavy mesons and baryons: experimental evidence. Rev. Mod. Phys. **90**, 015003 (2018). https://doi.org/10.1103/RevModPhys.90.015003
9. Y.S. Kalashnikova, A.V. Nefediev, X(3872) in the molecular model. Phys. Usp. **62**, 568–595 (2019). https://doi.org/10.3367/UFNe.2018.08.038411
10. N. Brambilla, S. Eidelman, C. Hanhart et al., The *XYZ* states: experimental and theoretical status and perspectives. Phys. Rep. **873**, 1–154 (2020). https://doi.org/10.1016/j.physrep.2020.05.001
11. F.K. Guo, X.H. Liu, S. Sakai, Threshold cusps and triangle singularities in hadronic reactions. Prog. Part. Nucl. Phys. **112**, 103757 (2020). https://doi.org/10.1016/j.ppnp.2020.103757
12. G. Yang, J. Ping, J. Segovia, Tetra- and penta-quark structures in the constituent quark model. Symmetry **12**, 1869 (2020). https://doi.org/10.3390/sym12111869
13. H.X. Chen, W. Chen, X. Liu et al., An updated review of the new hadron states. Rep. Prog. Phys. **86**, 026201 (2023). https://doi.org/10.1088/1361-6633/aca3b6
14. M. Mai, U.G. Meißner, C. Urbach, Towards a theory of hadron resonances. Phys. Rep. **1001**, 2248 (2023). https://doi.org/10.1016/j.physrep.2022.11.005
15. M.Z. Liu, Y.W. Pan, Z.W. Liu et al., Three ways to decipher the nature of exotic hadrons: multiplets, three-body hadronic molecules, and correlation functions. arXiv:2404.06399
16. S.K. Choi, S.L. Olsen, K. Abe et al., Observation of a narrow charmonium-like state in exclusive $B^\pm \to K^\pm \pi^+ \pi^- J/\psi$ decays.

Phys. Rev. Lett. **91**, 262001 (2003). https://doi.org/10.1103/PhysRevLett.91.262001

17. S.K. Choi, S.L. Olsen, I. Adachi et al., Observation of a resonance-like structure in the $pi^{\pm}\psi'$ mass distribution in exclusive $B \rightarrow K\pi^{\pm}\psi'$ decays. Phys. Rev. Lett. **100**, 142001 (2008). https://doi.org/10.1103/PhysRevLett.100.142001

18. A. Bondar et al., Observation of two charged bottomonium-like resonances in Y(5S) decays. Phys. Rev. Lett. **108**, 122001 (2012). https://doi.org/10.1103/PhysRevLett.108.122001

19. B. Aubert et al., Observation of a broad structure in the $\pi^+\pi^- J/\psi$ mass spectrum around $4.26 - GeV/c^2$. Phys. Rev. Lett. **95**, 142001 (2005). https://doi.org/10.1103/PhysRevLett.95.142001

20. R. Aaij et al., Observation of $J/\psi p$ resonances consistent with pentaquark states in $\Lambda_b^0 \rightarrow J/\psi K^- p$ decays. Phys. Rev. Lett. **115**, 072001 (2015). https://doi.org/10.1103/PhysRevLett.115.072001

21. R. Aaij et al., Determination of the X(3872) meson quantum numbers. Phys. Rev. Lett. **110**, 222001 (2013). https://doi.org/10.1103/PhysRevLett.110.222001

22. S. Navas et al., Review of particle physics. Phys. Rev. D **110**, 030001 (2024). https://doi.org/10.1103/PhysRevD.110.030001

23. C. Hanhart, Y.S. Kalashnikova, A.V. Nefediev, Lineshapes for composite particles with unstable constituents. Phys. Rev. D **81**, 094028 (2010). https://doi.org/10.1103/PhysRevD.81.094028

24. R. Aaij et al., Study of the lineshape of the $\chi_{c1}(3872)$ state. Phys. Rev. D **102**, 092005 (2020). https://doi.org/10.1103/PhysRevD.102.092005

25. M. Ablikim et al., Coupled-channel analysis of the $\chi c1(3872)$ line shape with BESIII data. Phys. Rev. Lett. **132**, 151903 (2024). https://doi.org/10.1103/PhysRevLett.132.151903

26. J.M. Dias, T. Ji, X.K. Dong et al., A model-independent analysis of the isospin breaking in the X(3872)→J/ψπ⁺π⁻ and X(3872)→J/ψπ⁺π⁰π⁻ decays. arXiv:2409.13245

27. J.P. Lees et al., Measurements of the absolute branching fractions of $B^{\pm} \rightarrow K^{\pm} X_{c\bar{c}}$. Phys. Rev. Lett. **124**, 152001 (2020). https://doi.org/10.1103/PhysRevLett.124.152001

28. C. Li, C.Z. Yuan, Determination of the absolute branching fractions of X(3872) decays. Phys. Rev. D **100**, 094003 (2019). https://doi.org/10.1103/PhysRevD.100.094003

29. N.A. Tornqvist, Isospin breaking of the narrow charmonium state of Belle at 3872-MeV as a deuson. Phys. Lett. B **590**, 209–215 (2004). https://doi.org/10.1016/j.physletb.2004.03.077

30. N.A. Tornqvist, From the deuteron to deusons, an analysis of deuteron - like meson meson bound states. Z. Phys. C **61**, 525–537 (1994). https://doi.org/10.1007/BF01413192

31. L. Maiani, F. Piccinini, A.D. Polosa et al., Diquark-antidiquarks with hidden or open charm and the nature of X(3872). Phys. Rev. D **71**, 014028 (2005). https://doi.org/10.1103/PhysRevD.71.014028

32. R. Aaij, A.S.W. Abdelmotteleb, C. Abellan Beteta et al., Probing the nature of the $\chi_{c1}(3872)$ state using radiative decays. arXiv: org/abs/2406.17006

33. R. Aaij, B. Adeva, M. Adinolfi et al., Evidence for the decay $X(3872) \rightarrow \psi(2S)\gamma$. Nucl. Phys. B **886**, 665–680 (2014). https://doi.org/10.1016/j.nuclphysb.2014.06.011

34. V. Bhardwaj, K. Trabelsi, J.B. Singh et al., Observation of $X(3872) \rightarrow J/\psi\gamma$ and search for $X(3872) \rightarrow \psi'\gamma$ in B decays. Phys. Rev. Lett. **107**, 091803 (2011). https://doi.org/10.1103/PhysRevLett.107.091803

35. B. Aubert, M. Bona, Y. Karyotakis et al., Evidence for $X(3872) \rightarrow \psi_{2S}\gamma$ in $B^{\pm} \rightarrow X_{3872}K^{\pm}$ decays, and a study of $B \rightarrow c\bar{c}\gamma K$. Phys. Rev. Lett. **102**, 132001 (2009). https://doi.org/10.1103/PhysRevLett.102.132001

36. M. Ablikim, M. N. Achasov, P. Adlarson et al., Study of open-charm decays and radiative transitions of the X(3872). Phys.

37. M. Ablikim, M. N. Achasov, S. Ahmed et al., Precise measurement of the $e^+e^- \rightarrow \pi^+\pi^- J/\psi$ cross section at center-of-mass energies from 3.77 to 4.60 GeV. Phys. Rev. Lett. **118**, 092001 (2017). https://doi.org/10.1103/PhysRevLett.118.092001

38. L. von Detten, V. Baru, C. Hanhart et al., How many vector charmonium(-like) states sit in the energy range from 4.2 to 4.35 GeV? Phys. Rev. D **109**, 116002 (2024). https://doi.org/10.1103/PhysRevD.109.116002

39. M. Ablikim, M. N. Achasov, P. Adlarson et al., Observation of a vector charmoniumlike State at 4.7 GeV/c² and Search for Zcs in e + e− → K + K − J/ψ. Phys. Rev. Lett. **131**, 211902 (2023). https://doi.org/10.1103/PhysRevLett.131.211902

40. M. Ablikim, M. N. Achasov, P. Adlarson et al., Observation of the Y(4230) and evidence for a new vector charmonium-like state Y(4710) in e + e− → KS0KS0J/ψ. Phys. Rev. D **107**, 092005 (2023). https://doi.org/10.1103/PhysRevD.107.092005

41. B. Aubert, M. Bona, Y. Karyotakis et al., Search for the Z(4430)- at BABAR. Phys. Rev. D **79**, 112001 (2009). https://doi.org/10.1103/PhysRevD.79.112001

42. R. Aaij, B. Adeva, M. Adinolfi et al., Observation of the resonant character of the Z(4430)⁻ state. Phys. Rev. Lett. **112**, 222002 (2014). https://doi.org/10.1103/PhysRevLett.112.222002

43. Z.Q. Liu, C.P. Shen, C.Z. Yuan et al., Study of e^+e^- ß $^{+-}J/$ and Observation of a Charged Charmoniumlike State at Belle. Phys. Rev. Lett. **110**, 252002 (2013). https://doi.org/10.1103/PhysRevLett.110.252002

44. M. Ablikim, M.N. Achasov, X.C. Ai et al., Observation of a Charged charmoniumlike structure in $e^+e^- \rightarrow \pi^+\pi^- J/\psi$ at $\sqrt{s}$ =4.26 GeV. Phys. Rev. Lett. **110**, 252001 (2013). https://doi.org/10.1103/PhysRevLett.110.252001

45. M. Ablikim, M.N. Achasov, O. Albayrak et al., Observation of a charged charmoniumlike structure $Z_c(4020)$ and Search for the $Z_c(3900)$ in e⁺e⁻ → π⁺π⁻h_c. Phys. Rev. Lett. **111**, 242001 (2013). https://doi.org/10.1103/PhysRevLett.111.242001

46. R. Mizuk, R. Chistov, I. Adachi et al., Observation of two resonance-like structures in the pi+ chi(c1) mass distribution in exclusive anti-B0 –> K- pi+ chi(c1) decays. Phys. Rev. D **78**, 072004 (2008). https://doi.org/10.1103/PhysRevD.78.072004

47. M. Ablikim, M. N. Achasov, P. Adlarson et al., Observation of a near-threshold structure in the K^+ recoil-mass spectra in $e^+e^- \rightarrow K^+(D_s^- D^{*0} + D_s^{*-}D^0)$. Phys. Rev. Lett. **126**, 102001 (2021). https://doi.org/10.1103/PhysRevLett.126.102001

48. R. Aaij, C. Abellán Beteta, T. Ackernley et al., Observation of new resonances decaying to $J/\psi K^+$ and $J/\psi\phi$. Phys. Rev. Lett. **127**, 082001 (2021). https://doi.org/10.1103/PhysRevLett.127.082001

49. Y.H. Chen, M.L. Du, F.K. Guo, Precise determination of the pole position of the exotic Z_c(3900). Sci. China Phys. Mech. Astron. **67**, 291011 (2024). https://doi.org/10.1007/s11433-023-2408-1

50. C. Hanhart, Important step towards an understanding of the exotic zc(3900). Sci. China Phys. Mech. Astron. **67**, 291031 (2024). https://doi.org/10.1007/s11433-024-2426-0

51. V.M. Abazov, B. Abbott, B.S. Acharya et al., Evidence for $Z_c^{\pm}$ (3900) in semi-inclusive decays of *b*-flavored hadrons. Phys. Rev. D **98**, 052010 (2018). https://doi.org/10.1103/PhysRevD.98.052010

52. V.M. Abazov, B. Abbott, B.S. Acharya et al., Properties of $Z_c^{\pm}$ (3900) produced in p p̄ collision. Phys. Rev. D **100**, 012005 (2019). https://doi.org/10.1103/PhysRevD.100.012005

53. T. Nakano et al., Evidence for a narrow S = +1 baryon resonance in photoproduction from the neutron. Phys. Rev. Lett. **91**, 012002 (2003). https://doi.org/10.1103/PhysRevLett.91.012002

54. R. Aaij et al., Observation of a narrow pentaquark state, $P_c(4312)^+$, and of two-peak structure of the $P_c(4450)^+$. Phys. Rev. Lett. **122**, 222001 (2019). https://doi.org/10.1103/PhysRevLett.122.222001

55. M.L. Du, V. Baru, F.K. Guo et al., Interpretation of the LHCb P_c states as hadronic molecules and hints of a narrow $P_c(4380)$. Phys. Rev. Lett. **124**, 072001 (2020). https://doi.org/10.1103/PhysRevLett.124.072001

56. R. Aaij, C. Abellán Beteta, T. Ackernley et al., First observation of the decay $\Lambda_b^0 \to \eta_c(1S)pK^-$. Phys. Rev. D **102**, 112012 (2020). https://doi.org/10.1103/PhysRevD.102.112012

57. R. Aaij, LHCb Collaboration, Evidence of a $J/\psi\Lambda$ structure and observation of excited Ξ^- states in the $\Xi_b^- \to J/\psi\Lambda K^-$ decay. Sci. Bull. **66**, 1278–1287 (2021). https://doi.org/10.1016/j.scib.2021.02.030

58. R. Aaij, A. S. W. Abdelmotteleb, C. Abellan Beteta et al., Observation of a J/ψΛ resonance consistent with a strange pentaquark candidate in B− → J/ψΛp− decays. Phys. Rev. Lett. **131**, 031901 (2023). https://doi.org/10.1103/PhysRevLett.131.031901

59. K.T. Chao, The S wave $Q\bar{Q}q\bar{q}$ states in the adiabatic approximation. Nucl. Phys. B **183**, 435–444 (1981). https://doi.org/10.1016/0550-3213(81)90143-7

60. R. Aaij, LHCb Collaboration, Observation of an exotic narrow doubly charmed tetraquark. Nat. Phys. **18**, 751–754 (2022). https://doi.org/10.1038/s41567-022-01614-y

61. R. Aaij, LHCb collaboration, Study of the doubly charmed tetraquark T_{cc}^+. Nat. Commun. **13**, 3351 (2022). https://doi.org/10.1038/s41467-022-30206-w

62. E.V. Shuryak, Quantum chromodynamics and the theory of superdense matter. Phys. Rep. **61**, 71–158 (1980). https://doi.org/10.1016/0370-1573(80)90105-2

63. J. Chen, X. Dong, X.H. He et al., Properties of the QCD matter: review of selected results from the relativistic heavy ion collider beam energy scan (RHIC BES) program. Nucl. Sci. Tech. **35**, 214 (2024). https://doi.org/10.1007/s41365-024-01591-2

64. Q.Y. Shou, Y.G. Ma, S. Zhang et al., Properties of the QCD matter: a review of selected results from the ALICE experiment. Nucl. Sci. Tech. **35**, 219 (2024). https://doi.org/10.1007/s41365-024-01583-2

65. B.I. Abelev, M.M. Aggarwal, Z. Ahammed et al., Observation of an antimatter hypernucleus. Science **328**, 58–62 (2010). https://doi.org/10.1126/science.1183980

66. H. Agakishiev, The STAR Collaboration, Observation of the antimatter helium-4 nucleus. Nature **473**, 353 (2011). https://doi.org/10.1038/nature10079

67. L. Adamczyk, The STAR Collaboration, Measurement of interaction between antiprotons. Nature **527**, 345–348 (2015). https://doi.org/10.1038/nature15724

68. J. Adam, D. Adamová, M.M. Aggarwal et al., $^3_\Lambda\text{H}$ and $^3_{\bar{\Lambda}}\overline{\text{H}}$ production in Pb-Pb collisions at $\sqrt{s_{NN}} = 2.76$ TeV. Phys. Lett. B **754**, 360–372 (2016). https://doi.org/10.1016/j.physletb.2016.01.040

69. S. Acharya, D. Adamová, J. Adolfsson et al., Production of ^{4}He and $^4\overline{\text{He}}$ in Pb-Pb collisions at $\sqrt{s_{NN}} = 2.76$ TeV at the LHC. Nucl. Phys. A **971**, 1–20 (2018). https://doi.org/10.1016/j.nuclphysa.2017.12.004

70. J. Adam, The STAR Collaboration, Measurement of the mass difference and the binding energy of the hypertriton and antihypertriton. Nat. Phys. **16**, 409–412 (2020). https://doi.org/10.1038/s41567-020-0799-7

71. M. Abdulhamid, STAR Collaboration, Observation of the antimatter hypernucleus $^4_{\bar{\Lambda}}\overline{\text{H}}$. Nature **632**, 1026–1031 (2024). https://doi.org/10.1038/s41586-024-07823-0

72. J. Chen, D. Keane, Y.G. Ma et al., Antinuclei in heavy-ion collisions. Phys. Rep. **760**, 1–39 (2018). https://doi.org/10.1016/j.physrep.2018.07.002

73. S. Cho, T. Furumoto, T. Hyodo et al., Identifying multi-quark hadrons from heavy ion collisions. Phys. Rev. Lett. **106**, 212001 (2011). https://doi.org/10.1103/PhysRevLett.106.212001

74. J. Chen, X. Dong, Y.G. Ma et al., Measurements of the lightest hypernucleus (HΛ3): progress and perspective. Sci. Bull. **68**, 3252–3260 (2023). https://doi.org/10.1016/j.scib.2023.11.045

75. M. Danysz, J. Pniewski, Delayed disintegration of a heavy nuclear fragment: I. Philos. Mag. **44**, 348 (1953). https://doi.org/10.1080/14786440308520318

76. S. Acharya et al., Measurement of the lifetime and Λ separation energy of HΛ3. Phys. Rev. Lett. **131**, 102302 (2023). https://doi.org/10.1103/PhysRevLett.131.102302

77. D.N. Liu, C.M. Ko, Y.G. Ma et al., Softening of the hypertriton transverse momentum spectrum in heavy-ion collisions. Phys. Lett. B **855**, 138855 (2024). https://doi.org/10.1016/j.physletb.2024.138855

78. N. Shah, Y.G. Ma, J.H. Chen et al., Production of multistrange hadrons, light nuclei and hypertriton in central Au+Au collisions at $\sqrt{s_{NN}} = 11.5$ and 200 GeV. Phys. Lett. B **754**, 6–10 (2016). https://doi.org/10.1016/j.physletb.2016.01.005

79. T. Shao, J. Chen, C.M. Ko et al., Enhanced production of strange baryons in high-energy nuclear collisions from a multiphase transport model. Phys. Rev. C **102**, 014906 (2020). https://doi.org/10.1103/PhysRevC.102.014906

80. S. Zhang, Y.G. Ma, Ω-dibaryon production with hadron interaction potential from the lattice QCD in relativistic heavy-ion collisions. Phys. Lett. B **811**, 135867 (2020). https://doi.org/10.1016/j.physletb.2020.135867

81. L. Zhang, S. Zhang, Y.G. Ma, Production of ΩNN and ΩΩN in ultra-relativistic heavy-ion collisions. Eur. Phys. J. C **82**, 416 (2022). https://doi.org/10.1140/epjc/s10052-022-10336-7

82. Y.G. Ma, Hypernuclei as a laboratory to test hyperon-nucleon interactions. Nucl. Sci. Tech. **34**, 97 (2023). https://doi.org/10.1007/s41365-023-01248-6

83. L. Adamczyk, J. K. Adkins, G. Agakishiev et al., ΛΛ correlation function in Au+Au collisions at $\sqrt{s_{NN}} = 200$ GeV. Phys. Rev. Lett. **114**, 022301 (2015). https://doi.org/10.1103/PhysRevLett.114.022301

84. S. Acharya, D. Adamová, S.P. Adhya et al., Study of the Λ-Λ interaction with femtoscopy correlations in pp and p-Pb collisions at the LHC. Phys. Lett. B **797**, 134822 (2019). https://doi.org/10.1016/j.physletb.2019.134822

85. A.M. Sirunyan, A. Tumasyan, W. Adam et al., Evidence for X(3872) in Pb-Pb collisions and studies of its prompt production at $\sqrt{s_{NN}}$=5.02 TeV. Phys. Rev. Lett. **128**, 032001 (2022). https://doi.org/10.1103/PhysRevLett.128.032001

86. S. Chatrchyan, V. Khachatryan, A.M. Sirunyan et al., Observation of sequential upsilon suppression in PbPb collisions. Phys. Rev. Lett. **109**, 222301 (2012). https://doi.org/10.1103/PhysRevLett.109.222301

87. A. Tumasyan, W. Adam, J. W. Andrejkovic et al., Observation of the Υ(3S) meson and suppression of Υ states in Pb-Pb collisions at $\sqrt{s_{NN}} = 5.02$ TeV. Phys. Rev. Lett. **133**, 022302 (2024). https://doi.org/10.1103/PhysRevLett.133.022302

88. V. Khachatryan, A.M. Sirunyan, A. Tumasyan et al., Suppression of Υ(1S), Υ(2S) and Υ(3S) production in PbPb collisions at $\sqrt{s_{NN}} = 2.76$ TeV. Phys. Lett. B **770**, 357–379 (2017). https://doi.org/10.1016/j.physletb.2017.04.031

89. A.M. Sirunyan, A. Tumasyan, W. Adam et al., Measurement of nuclear modification factors of Υ(1S), Υ(2S), and Υ(3S) mesons in PbPb collisions at $\sqrt{s_{NN}} = 5.02$ TeV. Phys. Lett. B

790, 270–293 (2019). https://doi.org/10.1016/j.physletb.2019.01.006

90. R. Aaij, A.S.W. Abdelmotteleb, C. Abellan Beteta et al., Modification of χc1(3872) and ψ(2S) production in pPb collisions at sNN=8.16 TeV. Phys. Rev. Lett. **132**, 242301 (2024). https://doi.org/10.1103/PhysRevLett.132.242301

91. R. Aaij, A.S.W. Abdelmotteleb, C. Abellan Beteta et al., Fraction of χc decays in prompt J/ψ production measured in pPb collisions at sNN=8.16 TeV. Phys. Rev. Lett. **132**, 102302 (2024). https://doi.org/10.1103/PhysRevLett.132.102302

92. R. Aaij, C. Abellan Beteta, B. Adeva et al., Measurement of the ratio of prompt χ_c to J/ψ production in *pp* collisions at $\sqrt{s} = 7$ TeV. Phys. Lett. B **718**, 431–440 (2012). https://doi.org/10.1016/j.physletb.2012.10.068

93. A. Tumasyan, W. Adam, J. W. Andrejkovic et al., Observation of the B_c^+ Meson in Pb-Pb and pp collisions at $\sqrt{s_{NN}}$=5.02 TeV and measurement of its nuclear modification factor. Phys. Rev. Lett. **128**, 252301 (2022). https://doi.org/10.1103/PhysRevLett.128.252301

94. D. Acosta, T. Affolder, M.H. Ahn et al., Observation of the narrow state $X(3872) \to J/\psi\pi^+\pi^-$ in $\bar{p}p$ collisions at $\sqrt{s} = 1.96$ TeV. Phys. Rev. Lett. **93**, 072001 (2004). https://doi.org/10.1103/PhysRevLett.93.072001

95. V.M. Abazov, B. Abbott, M. Abolins et al., Observation and properties of the $X(3872)$ decaying to $J/\psi\pi^+\pi^-$ in $p\bar{p}$ collisions at $\sqrt{s} = 1.96$ TeV. Phys. Rev. Lett. **93**, 162002 (2004). https://doi.org/10.1103/PhysRevLett.93.162002

96. R. Aaij, C. Abellan Beteta, B. Adeva et al., Observation of $X(3872)$ production in *pp* collisions at $\sqrt{s} = 7$ TeV. Eur. Phys. J. C **72**, 1972 (2012). https://doi.org/10.1140/epjc/s10052-012-1972-7

97. S. Chatrchyan, V. Khachatryan, A. M. Sirunyan et al., Measurement of the $X(3872)$ production cross section via decays to $J/\psi\pi^+\pi^-$ in *pp* collisions at $\sqrt{s} = 7$ TeV. JHEP **2013**, 154 (2013). https://doi.org/10.1007/JHEP04(2013)154

98. R. Aaij, C. Abellán Beteta, T. Ackernley et al., Observation of multiplicity dependent prompt $\chi_{c1}(3872)$ and $\psi(2S)$ production in *pp* collisions. Phys. Rev. Lett. **126**, 092001 (2021). https://doi.org/10.1103/PhysRevLett.126.092001

99. A. Abulencia, J. Adelman, T. Affolder et al., Analysis of the quantum numbers J^{PC} of the $X(3872)$. Phys. Rev. Lett. **98**, 132002 (2007). https://doi.org/10.1103/PhysRevLett.98.132002

100. T. Aaltonen, J. Adelman, T. Akimoto et al., Production of psi(2S) Mesons in p anti-p collisions at 1.96-TeV. Phys. Rev. D **80**, 031103 (2009). https://doi.org/10.1103/PhysRevD.80.031103

101. C. Bignamini, B. Grinstein, F. Piccinini et al., Is the X(3872) production cross section at Tevatron compatible with a hadron molecule interpretation? Phys. Rev. Lett. **103**, 162001 (2009). https://doi.org/10.1103/PhysRevLett.103.162001

102. P. Artoisenet, E. Braaten, Production of the X(3872) at the Tevatron and the LHC. Phys. Rev. D **81**, 114018 (2010). https://doi.org/10.1103/PhysRevD.81.114018

103. P. Artoisenet, E. Braaten, Estimating the production rate of loosely-bound hadronic molecules using event generators. Phys. Rev. D **83**, 014019 (2011). https://doi.org/10.1103/PhysRevD.83.014019

104. M. Albaladejo, F.K. Guo, C. Hanhart et al., Note on X(3872) production at hadron colliders and its molecular structure. Chin. Phys. C **41**, 121001 (2017). https://doi.org/10.1088/1674-1137/41/12/121001

105. E. Epelbaum, H.W. Hammer, U.G. Meissner, Modern theory of nuclear forces. Rev. Mod. Phys. **81**, 1773–1825 (2009). https://doi.org/10.1103/RevModPhys.81.1773

106. D. Gamermann, E. Oset, D. Strottman et al., Dynamically generated open and hidden charm meson systems. Phys. Rev. D **76**, 074016 (2007). https://doi.org/10.1103/PhysRevD.76.074016

107. X.K. Dong, F.K. Guo, B.S. Zou, A survey of heavy-antiheavy hadronic molecules. Prog. Phys. **41**, 65–93 (2021). https://doi.org/10.13725/j.cnki.pip.2021.02.001

108. F.Z. Peng, M.J. Yan, M. Pavon Valderrama, Heavy- and light-flavor symmetry partners of the Tcc+(3875), the X(3872), and the X(3960) from light-meson exchange saturation. Phys. Rev. D **108**, 114001 (2023). https://doi.org/10.1103/PhysRevD.108.114001

109. G.J. Wang, Z. Yang, J.J. Wu et al., New insight into the exotic states strongly coupled with the $D\bar{D}^*$ from the T_{cc}^+. Sci. Bull. **69**, 3036 (2024). https://doi.org/10.1016/j.scib.2024.07.012

110. J. Nieves, M.P. Valderrama, The heavy quark spin symmetry partners of the X(3872). Phys. Rev. D **86**, 056004 (2012). arXiv: 1204.2790, https://doi.org/10.1103/PhysRevD.86.056004

111. S. Chen, C. Shi, Y. Chen et al., Tcc+(3875) relevant DD* scattering from Nf=2 lattice QCD. Phys. Lett. B **833**, 137391 (2022). https://doi.org/10.1016/j.physletb.2022.137391

112. X.K. Dong, F.K. Guo, B.S. Zou, A survey of heavy–heavy hadronic molecules. Commun. Theor. Phys. **73**, 125201 (2021). https://doi.org/10.1088/1572-9494/ac27a2

113. A. Feijoo, W.H. Liang, E. Oset, D0D0π+ mass distribution in the production of the Tcc exotic state. Phys. Rev. D **104**, 114015 (2021). https://doi.org/10.1103/PhysRevD.104.114015

114. A. Nogga, C. Hanhart, Can one extract the pi-neutron scattering length from pi-deuteron scattering? Phys. Lett. B **634**, 210–213 (2006). https://doi.org/10.1016/j.physletb.2005.12.071

115. E. Braaten, M. Kusunoki, Factorization in the production and decay of the X(3872). Phys. Rev. D **72**, 014012 (2005). https://doi.org/10.1103/PhysRevD.72.014012

116. C. Meng, H. Han, K.T. Chao, X(3872) and its production at hadron colliders. Phys. Rev. D **96**, 074014 (2017). https://doi.org/10.1103/PhysRevD.96.074014

117. M. Butenschoen, Z.G. He, B.A. Kniehl, Deciphering the X(3872) via its polarization in prompt production at the CERN LHC. Phys. Rev. Lett. **123**, 032001 (2019). https://doi.org/10.1103/PhysRevLett.123.032001

118. A. Cisek, W. Schäfer, A. Szczurek, Structure and production mechanism of the enigmatic X(3872) in high-energy hadronic reactions. Eur. Phys. J. C **82**, 1062 (2022). https://doi.org/10.1140/epjc/s10052-022-11029-x

119. S. Weinberg, Evidence that the deuteron is not an elementary particle. Phys. Rev. **137**, B672–B678 (1965). https://doi.org/10.1103/PhysRev.137.B672

120. E. Braaten, M. Kusunoki, Low-energy universality and the new charmonium resonance at 3870-MeV. Phys. Rev. D **69**, 074005 (2004). https://doi.org/10.1103/PhysRevD.69.074005

121. F.K. Guo, U.G. Meißner, W. Wang et al., Production of the bottom analogs and the spin partner of the X(3872) at hadron colliders. Eur. Phys. J. C **74**, 3063 (2014). https://doi.org/10.1140/epjc/s10052-014-3063-4

122. G.P. Lepage, S.J. Brodsky, Exclusive processes in perturbative quantum chromodynamics. Phys. Rev. D **22**, 2157 (1980). https://doi.org/10.1103/PhysRevD.22.2157

123. M.B. Voloshin, Constituent counting rule for exclusive production of heavy quarkoniumlike exotic resonance and a light hadron. Phys. Rev. D **94**, 074042 (2016). https://doi.org/10.1103/PhysRevD.94.074042

124. J. Adam, D. Adamová, M.M. Aggarwal et al., Production of light nuclei and anti-nuclei in pp and Pb-Pb collisions at energies available at the CERN Large Hadron Collider. Phys. Rev. C **93**, 024917 (2016). https://doi.org/10.1103/PhysRevC.93.024917

125. A. Esposito, A.L. Guerrieri, L. Maiani et al., Observation of light nuclei at ALICE and the X(3872) conundrum. Phys. Rev. D **92**, 034028 (2015). https://doi.org/10.1103/PhysRevD.92.034028

126. S. Acharya, D. Adamová, G. Aglieri Rinella et al., Observation of abnormal suppression of f0(980) production in p-Pb collisions at $\sqrt{s_{NN}}$ = 5.02 TeV. Phys. Lett. B **853**, 138665 (2024). https://doi.org/10.1016/j.physletb.2024.138665

127. J.D. Weinstein, N. Isgur, K anti-K molecules. Phys. Rev. D **41**, 2236 (1990). https://doi.org/10.1103/PhysRevD.41.2236

128. V. Baru, J. Haidenbauer, C. Hanhart et al., Evidence that the a(0) (980) and f(0)(980) are not elementary particles. Phys. Lett. B **586**, 53–61 (2004). https://doi.org/10.1016/j.physletb.2004.01.088

129. A. Hayrapetyan, A. Tumasyan, W. Adam et al., Elliptic anisotropy measurement of the f_0(980) hadron in proton-lead collisions and evidence for its quark-antiquark composition. arXiv: 2312.17092

130. A. Esposito, E.G. Ferreiro, A. Pilloni et al., The nature of X(3872) from high-multiplicity pp collisions. Eur. Phys. J. C **81**, 669 (2021). https://doi.org/10.1140/epjc/s10052-021-09425-w

131. E. Braaten, L.P. He, K. Ingles et al., Production of X(3872) at high multiplicity. Phys. Rev. D **103**, L071901 (2021). https://doi.org/10.1103/PhysRevD.103.L071901

132. R.H. Dalitz, S.F. Tuan, A possible resonant state in pion-hyperon scattering. Phys. Rev. Lett. **2**, 425–428 (1959). https://doi.org/10.1103/PhysRevLett.2.425

133. N. Kaiser, P.B. Siegel, W. Weise, Chiral dynamics and the S11 (1535) nucleon resonance. Phys. Lett. B **362**, 23–28 (1995). https://doi.org/10.1016/0370-2693(95)01203-3

134. J.A. Oller, U.G. Meißner, Chiral dynamics in the presence of bound states: Kaon nucleon interactions revisited. Phys. Lett. B **500**, 263–272 (2001). https://doi.org/10.1016/S0370-2693(01)00078-8

135. R.L. Jaffe, Multi-quark hadrons. 2 methods. Phys. Rev. D **15**, 281 (1977). https://doi.org/10.1103/PhysRevD.15.281

136. P. Adlarson, W. Augustyniak, W. Bardan et al., Evidence for a new resonance from polarized neutron-proton scattering. Phys. Rev. Lett. **112**, 202301 (2014). https://doi.org/10.1103/PhysRevLett.112.202301

137. A. Gal, H. Garcilazo, Three-body calculation of the delta-delta dibaryon candidate D(03) at 2.37 GeV. Phys. Rev. Lett. **111**, 172301 (2013). https://doi.org/10.1103/PhysRevLett.111.172301

138. M. Bashkanov, S.J. Brodsky, H. Clement, Novel six-quark hidden-color dibaryon states in QCD. Phys. Lett. B **727**, 438–442 (2013). https://doi.org/10.1016/j.physletb.2013.10.059

139. H. Huang, J. Ping, F. Wang, Dynamical calculation of the $\Delta\Delta$ dibaryon candidates. Phys. Rev. C **89**, 034001 (2014). https://doi.org/10.1103/PhysRevC.89.034001

140. T. Yamaga, S. Ajimura, H. Asano et al., Measurement of the mesonic decay branch of the K⁻NN quasibound state. Phys. Rev. C **110**, 014002 (2024). https://doi.org/10.1103/PhysRevC.110.014002

141. C. Hanhart, Meson production in nucleon-nucleon collisions close to the threshold. Phys. Rep. **397**, 155–256 (2004). https://doi.org/10.1016/j.physrep.2004.03.007

142. P. Moskal, M. Wolke, A. Khoukaz et al., Close-to-threshold meson production in hadronic interactions. Prog. Part. Nucl. Phys. **49**, 1 (2002). https://doi.org/10.1016/S0146-6410(02)00143-6

143. Z. Ouyang, J.J. Xie, B.S. Zou et al., Role of the N*(1440) resonance in the pp –> pn pi+ reaction. Nucl. Phys. A **821**, 220–234 (2009). https://doi.org/10.1016/j.nuclphysa.2009.02.010

144. J.J. Wu, Z. Ouyang, B.S. Zou, Proposal for studying N* resonances with anti-p p –> anti-p n pi+ reaction. Phys. Rev. C **80**, 045211 (2009). https://doi.org/10.1103/PhysRevC.80.045211

145. K. Tsushima, A. Sibirtsev, A.W. Thomas et al., Resonance model study of kaon production in baryon baryon reactions for heavy ion collisions. Phys. Rev. C **59**, 369–387 (1999). https://doi.org/10.1103/PhysRevC.59.369

146. J.J. Xie, B.S. Zou, The Role of Delta++*(1620) resonances in pp –> nK+ Sigma+ reaction and its important implications. Phys. Lett. B **649**, 405–412 (2007). https://doi.org/10.1016/j.physletb.2007.04.035

147. Q.F. Lü, D.M. Li, Near-threshold η production in pp collisions. Chin. Phys. C **39**, 113104 (2015). https://doi.org/10.1088/1674-1137/39/11/113104

148. R. Münzer et al., Determination of N* amplitudes from associated strangeness production in p+p collisions. Phys. Lett. B **785**, 574–580 (2018). https://doi.org/10.1016/j.physletb.2018.08.068

149. B.C. Liu, B.S. Zou, Mass and K lambda coupling of N*(1535). Phys. Rev. Lett. **96**, 042002 (2006). https://doi.org/10.1103/PhysRevLett.96.042002

150. J.J. Wu, R. Molina, E. Oset et al., Prediction of narrow N* and Λ* resonances with hidden charm above 4 GeV. Phys. Rev. Lett. **105**, 232001 (2010). https://doi.org/10.1103/PhysRevLett.105.232001

151. H. Clement, On the history of dibaryons and their final observation. Prog. Part. Nucl. Phys. **93**, 195 (2017). https://doi.org/10.1016/j.ppnp.2016.12.004

152. R. Molina, N. Ikeno, E. Oset, Sequential single pion production explaining the dibaryon d*(2380) peak*. Chin. Phys. C **47**, 041001 (2023). https://doi.org/10.1088/1674-1137/acb0b7

153. X.Q. Yuan, Z.Y. Zhang, Y.W. Yu et al., Deltaron dibaryon structure in chiral SU(3) quark model. Phys. Rev. C **60**, 045203 (1999). https://doi.org/10.1103/PhysRevC.60.045203

154. L.R. Dai, Delta Delta dibaryon structure in extended chiral SU(3) quark model. Chin. Phys. Lett. **22**, 2204–2206 (2005). https://doi.org/10.1088/0256-307X/22/9/018

155. L. Dai, Y. Wang, L. Chen et al., The role of the hidden color channel in some interesting dibaryon candidates. Symmetry **15**, 446 (2023). https://doi.org/10.3390/sym15020446

156. C. Wilkin, The legacy of the experimental hadron physics programme at COSY. Eur. Phys. J. A **53**, 114 (2017). https://doi.org/10.1140/epja/i2017-12295-4

157. J.J. Xie, H.X. Chen, E. Oset, The pp -> p ΛK^+ and pp – > p $\Sigma^0 K^+$ reactions with chiral dynamics. Phys. Rev. C **84**, 034004 (2011). https://doi.org/10.1103/PhysRevC.84.034004

158. V. Komarov, D. Tsirkov, T. Azaryan et al., Evidence for excitation of two resonance states in the isovector two-baryon system with a mass of 2.2 GeV/c^2. Phys. Rev. C **93**, 065206 (2016). https://doi.org/10.1103/PhysRevC.93.065206

159. H. Clement, T. Skorodko, E. Doroshkevich, Possibility of dibaryon formation near the N*(1440)N threshold: reexamination of isoscalar single-pion production. Phys. Rev. C **106**, 065204 (2022). https://doi.org/10.1103/PhysRevC.106.065204

160. V.I. Kukulin, O.A. Rubtsova, M.N. Platonova et al., Nature of S -wave NN interaction and dibaryon production at nucleonic resonance thresholds. Eur. Phys. J. A **56**, 229 (2020). https://doi.org/10.1140/epja/s10050-020-00236-3

161. M.G. Albrow, T.D. Coughlin, J.R. Forshaw, Central exclusive particle production at high energy hadron colliders. Prog. Part. Nucl. Phys. **65**, 149–184 (2010). https://doi.org/10.1016/j.ppnp.2010.06.001

162. P. Lebiedowicz, O. Nachtmann, A. Szczurek, Towards a complete study of central exclusive production of K^+K^- pairs in proton-proton collisions within the tensor Pomeron approach. Phys.

Rev. D **98**, 014001 (2018). https://doi.org/10.1103/PhysRevD.98.014001

163. A. Szczurek, P. Lebiedowicz, Exclusive scalar f0(1500) meson production for energy ranges available at the GSI Facility for Antiproton and Ion Research (GSI-FAIR) and at the Japan Proton Accelerator Research Complex (J-PARC). Nucl. Phys. A **826**, 101–130 (2009). https://doi.org/10.1016/j.nuclphysa.2009.05.072

164. M.V.T. Machado, Investigating the central diffractive f0(980) and f2(1270) meson production at the LHC. Phys. Rev. D **86**, 014029 (2012). https://doi.org/10.1103/PhysRevD.86.014029

165. P. Lebiedowicz, R. Maciuła, A. Szczurek, Production of $f_0(980)$ meson at the LHC: color evaporation versus color-singlet gluon-gluon fusion. Phys. Lett. B **806**, 135475 (2020). https://doi.org/10.1016/j.physletb.2020.135475

166. D. Ronchen, M. Doring, F. Huang et al., Coupled-channel dynamics in the reactions piN -> piN, etaN, KLambda, KSigma. Eur. Phys. J. A **49**, 44 (2013). https://doi.org/10.1140/epja/i2013-13044-5

167. A. Matsuyama, T. Sato, T.S.H. Lee, Dynamical coupled-channel model of meson production reactions in the nucleon resonance region. Phys. Rep. **439**, 193–253 (2007). https://doi.org/10.1016/j.physrep.2006.12.003

168. D. Sadasivan, A. Alexandru, H. Akdag et al., Pole position of the a1(1260) resonance in a three-body unitary framework. Phys. Rev. D **105**, 054020 (2022). https://doi.org/10.1103/PhysRevD.105.054020

169. S.X. Nakamura, Q. Huang, J.J. Wu et al., Three-body unitary coupled-channel analysis on η(1405/1475). Phys. Rev. D **107**, L091505 (2023). https://doi.org/10.1103/PhysRevD.107.L091505

170. A. Ohnishi, S. Cho, T. Furumoto et al., Exotic hadrons and hadron-hadron interactions in heavy ion collisions. Nucl. Phys. A **914**, 377–386 (2013). https://doi.org/10.1016/j.nuclphysa.2013.01.083

171. S. Cho, T. Hyodo, D. Jido et al., Exotic hadrons from heavy ion collisions. Prog. Part. Nucl. Phys. **95**, 279–322 (2017). https://doi.org/10.1016/j.ppnp.2017.02.002

172. A. Ohnishi, K. Morita, K. Miyahara et al., Hadron–hadron correlation and interaction from heavy–ion collisions. Nucl. Phys. A **954**, 294–307 (2016). https://doi.org/10.1016/j.nuclphysa.2016.05.010

173. K.J. Sun, L.W. Chen, Analytical coalescence formula for particle production in relativistic heavy-ion collisions. Phys. Rev. C **95**, 044905 (2017). https://doi.org/10.1103/PhysRevC.95.044905

174. C.E. Fontoura, G. Krein, A. Valcarce et al., Production of exotic tetraquarks $QQ\bar{q}\bar{q}$ in heavy-ion collisions at the LHC. Phys. Rev. D **99**, 094037 (2019). https://doi.org/10.1103/PhysRevD.99.094037

175. H. Zhang, J. Liao, E. Wang et al., Deciphering the nature of X(3872) in heavy ion collisions. Phys. Rev. Lett. **126**, 012301 (2021). https://doi.org/10.1103/PhysRevLett.126.012301

176. A. Andronic, P. Braun-Munzinger, M.K. Köhler et al., Transverse momentum distributions of charmonium states with the statistical hadronization model. Phys. Lett. B **797**, 134836 (2019). https://doi.org/10.1016/j.physletb.2019.134836

177. Y. Hu, J. Liao, E. Wang et al., Production of doubly charmed exotic hadrons in heavy ion collisions. Phys. Rev. D **104**, L111502 (2021). https://doi.org/10.1103/PhysRevD.104.L111502

178. B. Chen, L. Jiang, X.H. Liu et al., X(3872) production in relativistic heavy-ion collisions. Phys. Rev. C **105**, 054901 (2022). https://doi.org/10.1103/PhysRevC.105.054901

179. B. Chen, M. Yang, G. Chen et al., Production of doubly charmed hadrons Ξcc++ and Tcc+ in relativistic heavy-ion collisions.

180. S. Cho, S.H. Lee, Hadronic effects on the X(3872) meson abundance in heavy ion collisions. Phys. Rev. C **88**, 054901 (2013). https://doi.org/10.1103/PhysRevC.88.054901

181. L.M. Abreu, K.P. Khemchandani, A. Martinez Torres et al., X(3872) production and absorption in a hot hadron gas. Phys. Lett. B **761**, 303–309 (2016). https://doi.org/10.1016/j.physletb.2016.08.050

182. A. Martinez Torres, K.P. Khemchandani, F.S. Navarra et al., On X(3872) production in high energy heavy ion collisions. Phys. Rev. D **90**, 114023 (2014). https://doi.org/10.1103/PhysRevD.90.114023

183. J. Hong, S. Cho, T. Song et al., Hadronic effects on the $cc\bar{q}\bar{q}$ tetraquark state in relativistic heavy ion collisions. Phys. Rev. C **98**, 014913 (2018). https://doi.org/10.1103/PhysRevC.98.014913

184. B. Wu, X. Du, M. Sibila et al., X(3872) transport in heavy-ion collisions. Eur. Phys. J. A **57**, 122 (2021). https://doi.org/10.1140/epja/s10050-021-00623-4

185. M. Cleven, V.K. Magas, A. Ramos, X(3872) in a hot pion bath. Phys. Lett. B **799**, 135050 (2019). https://doi.org/10.1016/j.physletb.2019.135050

186. E. Braaten, L.P. He, K. Ingles et al., Thermal energy of a charm-meson molecule in a pion gas. JHEP **02**, 163 (2024). https://doi.org/10.1007/JHEP02(2024)163

187. E. Braaten, K. Ingles, J. Pickett, How the contact can produce snowballs from hell. arXiv: org/abs/2408.03935

188. L.M. Abreu, F.S. Navarra, H.P.L. Vieira, X(3872) to ψ(2S) yield ratio in heavy-ion collisions. Phys. Rev. D **110**, 014011 (2024). https://doi.org/10.1103/PhysRevD.110.014011

189. Y. Guo, X. Guo, J. Liao et al., Medium-assisted enhancement of χc1(3872) production from small to large colliding systems. Phys. Rev. C **110**, L021901 (2024). https://doi.org/10.1103/PhysRevC.110.L021901

190. J. Matthew Durham (LHCb), Modification of χ_{c1}(3872) and ψ(2S) production in *p*Pb collisions at $\sqrt{s_{NN}}$ = 8.16 TeV, conference report prepared for Quark Matter 2022, Krakow, Poland, April 4–10, 2022 (2022)

191. M.A. Lisa, S. Pratt, R. Soltz et al., Femtoscopy in relativistic heavy ion collisions. Ann. Rev. Nucl. Part. Sci. **55**, 357–402 (2005). arXiv: org/abs/nucl-ex/0505014 , https://doi.org/10.1146/annurev.nucl.55.090704.151533

192. K. Morita, S. Gongyo, T. Hatsuda et al., Probing ΩΩ and *p*Ω dibaryons with femtoscopic correlations in relativistic heavy-ion collisions. Phys. Rev. C **101**, 015201 (2020). https://doi.org/10.1103/PhysRevC.101.015201

193. S. Acharya, D. Adamová, A. Adler et al., Search for a common baryon source in high-multiplicity pp collisions at the LHC. Phys. Lett. B **811**, 135849 (2020). https://doi.org/10.1016/j.physletb.2020.135849

194. S. Acharya, D. Adamová, G. Aglieri Rinella et al., Common femtoscopic hadron-emission source in pp collisions at the LHC. arXiv: 2311.14527

195. M. Ablikim, M.N. Achasov, X.C. Ai et al., Observation of e+e− → γ X(3872) at BESIII. Phys. Rev. Lett. **112**, 092001 (2014). https://doi.org/10.1103/PhysRevLett.112.092001

Authors and Affiliations

Jin-Hui Chen[1,2] · **Feng-Kun Guo**[3,4,5,6] · **Yu-Gang Ma**[1,2] · **Cheng-Ping Shen**[1,2] · **Qi-Ye Shou**[1,2] · **Qian Wang**[6,7,8] · **Jia-Jun Wu**[4] · **Bing-Song Zou**[3,5,6,9]

✉ Feng-Kun Guo
  fkguo@itp.ac.cn

1   Key Laboratory of Nuclear Physics and Ion-beam Application (MOE), Institute of Modern Physics, Fudan University, Shanghai 200433, China

2   Shanghai Research Center for Theoretical Nuclear Physics, NSFC and Fudan University, Shanghai 200438, China

3   CAS Key Laboratory of Theoretical Physics, Institute of Theoretical Physics, Chinese Academy of Sciences, Beijing 100190, China

4   School of Physical Sciences, University of Chinese Academy of Sciences, Beijing 100049, China

5   Peng Huanwu Collaborative Center for Research and Education, Beihang University, Beijing 100191, China

6   Southern Center for Nuclear-Science Theory (SCNT), Institute of Modern Physics, Chinese Academy of Sciences, Huizhou 516000, China

7   Guangdong-Hong Kong Joint Laboratory of Quantum Matter, Guangdong Provincial Key Laboratory of Nuclear Science, Southern Nuclear Science Computing Center, South China Normal University, Guangzhou 510006, China

8   Key Laboratory of Atomic and Subatomic Structure and Quantum Control (MOE), Guangdong Basic Research Center of Excellence for Structure and Fundamental Interactions of Matter, Institute of Quantum Matter, South China Normal University, Guangzhou 510006, China

9   Department of Physics, Tsinghua University, Beijing 100084, China